THE ELECTRICAL AND PHOTOLUMINESCENCE CHARACTERISTICS OF THERMALLY DEPOSITED ALQ₃ FILMS

KOAY JAN YEONG

DISSERTATION SUBMITTED IN FULFILMENT

OF THE REQUIREMENTS

FOR THE DEGREE OF MASTER OF SCIENCE

DEPARTMENT OF PHYSICS

FACULTY OF SCIENCE

UNIVERSITY OF MALAYA

YEAR 2010

Acknowledgement

I would like to express my sincere thanks to my supervisor, Prof. Datin Dr. Saadah Abdul Rahman for her invaluable suggestions and encouragement. I also would like to express my deep gratitude to my beloved parents, Mr. Koay Geak Kiang and Mrs. Low Mui Yong for their constant support and encouragement during my studies in University of Malaya. Many thanks also go to the members of Solid State Research Laboratory, especially En. Khairul Anuar Bin Mat Sharif, Mr. Goh Boon Tong and Mr. Richard Ritikos for always being helpful and giving me useful advices in the lab. I also would like to say Thank You to everybody that have helped me but not mentioned above. It is incomplete for this acknowledgement without expressing my heartfelt thanks to my girlfriend, Miss Lee Sze Teng for her support, encouragement, co-operation and love throughout the preparation of this thesis.

UNIVERSITI MALAYA
ORIGINAL LITERARY WORK DECLARATION

Name of Candidate: **Koay Jan Yeong**   (I.C/Passport No: **820418-07-5143**)

Registration/Matric No: **SGR070045**

Name of Degree: **Master of Science**

Title of Project Paper/Research Report/Dissertation/Thesis ("this Work"):
The Electrical and Photoluminescence Characteristics of Thermally Deposited Alq$_3$ Films

Field of Study: **Low Dimensional Semiconductor**

I do solemnly and sincerely declare that:
(1) I am the sole author/writer of this Work;
(2) This Work is original;
(3) Any use of any work in which copyright exists was done by way of fair dealing and for permitted purposes and any excerpt or extract from, or reference to or reproduction of any copyright work has been disclosed expressly and sufficiently and the title of the Work and its authorship have been acknowledged in this Work;
(4) I do not have any actual knowledge nor do I ought reasonably to know that the making of this work constitutes an infringement of any copyright work;
(5) I hereby assign all and every rights in the copyright to this Work to the University of Malaya ("UM"), who henceforth shall be owner of the copyright in this Work and that any reproduction or use in any form or by any means whatsoever is prohibited without the written consent of UM having been first had and obtained;
(6) I am fully aware that if in the course of making this Work I have infringed any copyright whether intentionally or otherwise, I may be subject to legal action or any other action as may be determined by UM.

Candidate's Signature   Date:

Subscribed and solemnly declared before,

Witness's Signature   Date:
Name: **Saadah Abdul Rahman**
Designation: **Professor Datin Doctor**

Abstract

Low molecules organic materials are attracting much attention as a candidate for flat panel displays and semiconductor applications. The tris (8-hydroxyquinoline) aluminum (III) complex (Alq_3), is the most important and widely studied material. However, there are still many things which remain to be studied. In this work, the effects of various surface treatments using CH_4, He, Ar, O_2 plasma and UV/O_3 treatments on anode material surfaces (c-Si and ITO) have been studied on the photoluminescence and electrical properties of Alq_3 films prepared by vacuum evaporation technique using an in-house designed and built deposition system. Photoluminescence (PL) and current-voltage (*I-V*) measurements were done to investigate these properties. The PL results demonstrated that the PL peak intensity and peak position of the deposited film was effected by the surface treatments done on the anode material surfaces. The Fowler-Nordheim (FN) model was used on the *I-V* plots to estimate the barrier height of the deposited films. The results showed that threshold voltage (V_T), threshold current (J_T), OLEDs driving voltage (V_d) and barrier height (Φ_B) were effected on the various surface treatments done on the anode material surfaces. In general, the electrical and PL properties of Alq_3 films on ITO are enhanced with UV/O_3 treatment which is an establish technique used for cleaning ITO in $ITO/Alq_3/Al$ heterostructure. PL emission intensity of Alq_3 films on ITO substrates also is enhanced with increase in O_2 plasma treatment time on the ITO substrates. Electrical properties of $ITO/Alq_3/Al$ heterostructures improve with short duration O_2 plasma treatment time on the ITO but are downgraded for long treatment time. Short duration He and Ar and plasma treatments remove hydrocarbon contamination on the ITO and c-Si substrate surfaces and this has the effect of increasing hole injection in $ITO/Alq_3/Al$ and p-type c-Si/Alq_3/Al heterostructures. Long duration He and Ar plasma treatments on these substrates expose the treated substrate surface to prolonged ion bombardments producing a decrease in the PL emission intensity and hole injection in the ITO and c-Si anode heterostructures. The CH_4 plasma treatment produces adverse effects on the electrical and PL properties of Alq_3 films on these substrates as result of the formation of hydrocarbon layer.

Abstrak

Bahan organik yang bermolekul kecil telah menarik perhatian sebagai calon untuk penggunaan skrin paparan rata dan peranti elektronik. Tris (8-hydroxyquinoline) aluminum (III) complex (Alq$_3$) merupakan salah satu bahan yang paling penting dikaji secara meluas. Walau bagaimanpun, masih terdapat banyak aspek yang boleh dikaji. Dalam kajian ini, kesan-kesan daripada pelbagai rawatan atas permukaan bahan anod dengan menggunakan nyahcas daripada CH$_4$, He, Ar, O$_2$ dan UV/O$_3$ rawatan telah dikaji terhadap sifat fotoluminesen (PL) dan elektrik Alq$_3$ filem yang disedia daripada teknik penyejatan vacum yang menggunakan rekaan dan binaan sistem pemendapan sendirian. Pengukuran PL dan elektrik digunakan untuk mengkaji sifat-sifat tersebut. Keputusan PL menunjukkan bahawa puncak keamatan dan puncak kedudukan PL dipengaruhi oleh rawatan permukaan yang dijalankan atas permukaan bahan anod. Model Fowler-Nordheim telah digunakan atas plot *I-V* untuk menganggarkan ketinggian halangan termendap filem. Keputusan menunjukkan voltan ambang (V_T), arus ambang (J_T), voltan panduan OLEDs (V_d), dan ketinggian halangan (Φ_B) adalah dipengaruh oleh rawatan permukaan atas permukaan bahan anod. Umumnya, sifat elektrik dan PL filem Alq$_3$ pada ITO dipertingkatkan dengan rawatan UV/O$_3$ yang merupakan teknik yang digunakan untuk pembersihan ITO dalam ITO/Alq$_3$/Al struktur hetero. Keamatan pancaran PL filem Alq$_3$ atas substrat ITO juga dipertingkatkan dengan peningkatan jangka masa waktu rawatan plasma O$_2$ pada substrat ITO. Sifat elektrik dalam ITO/Alq$_3$/Al struktur hetero diperbaiki dengan waktu rawatan jangka masa pendek plasma O$_2$ pada ITO namun diturunkan dengan waktu rawatan jangka masa panjang. Waktu rawatan jangka masa pendek plasma He dan Ar menghilangkan pencemaran hidrokarbon di permukaan substrat ITO dan c-Si dan ini mempunyai kesan dalam meningkatkan suntikan lohong di ITO/Alq$_3$/Al dan c-Si/Alq$_3$/Al jenis-p dalam struktur hetero. Waktu rawatan jangka masa panjang plasma He and Ar pada substrat ini mendedahkan permukaan substrat yang dirawat terhadap pengeboman ion yang berpanjangan menyebabkan penurunan dalam keamatan pancaran PL dan suntikan lohong di ITO and c-Si dalam struktur hetero. Rawatan plasma CH$_4$ menghasilkan kesan yang sebaliknya pada sifat PL Alq$_3$ film pada substrat ini akibat dari pembentukan lapisan hidrokarbon.

Contents

List of Figures

List of Tables

Abbreviations

δ	dipole moment
π	valence band
χ	energy difference between vacuum level and Fermi level
π^*	conduction band
A	area
AFM	atomic force microscope
Alq_3	tris (8-hydroxyquinoline) aluminum (III)
Ar	argon
C:H	hydrocarbon
CF	fluorocarbon
CH_4	methane
c-Si	crystal silicon
E	electric field
EA	electron affinity
EL	electroluminescence
FN	Fowler-Nordheim
h	Planck's constant
He	helium
HOMO	highest occupied molecular orbital
I_{FN}	Fowler-Nordheim current
IP	ionization potential
ITO	indium tin oxide
I-V	current-voltage
j_e	electron current density without recombination
j_e'	electron current density reaching the anode without recombination
j_h	hole current density without recombination
j_h'	hole current density reaching the cathode without recombination
J_T	threshold current
LUMO	lowest unoccupied molecular orbital
m^*	effective mass of carriers

O_2	oxygen
OFET	organic field effect transistor
OLED	organic light-emitting diode
OSC	organic semiconductor
PL	photoluminescence
q	electronic charge
RF	radio frequency
UPS	ultra-violet photoelectron spectroscopy
UV/O_3	ultraviolet ozone
V	applied voltage
V_d	OLED driving voltage
V_T	threshold voltage
Φ_A	anode work function
Φ_B	barrier height
Φ_C	cathode work function
Φ_e	electron injection barrier
Φ_h	hole injection barrier

Chapter 1 Introduction

Since the 1970s controlled doping of conjugated polymers [*Chiang et al., (1977)*] has been successfully synthesized. This established the second important class of organic semiconductors (OSCs) and triggered the first applications of organic materials as conductive coating or photoreceptors in electro photography [*Borsenberger and Weiss, (1993)*].

As a result of this, an efficient photovoltaic cell incorporating an organic hetero-junction of p- and n-conducting materials [*Tang, (1986)*] was fabricated. The first successful fabrication of thin film transistors from conjugated polymers and oligomers [*Koezuka et al., (1987)*] as well as high-performance multilayer organic light-emitting diode (OLED) and electroluminescent (EL) diode devices from vacuum evaporated molecular films was reported by Tang and VanSlyke in 1980s [*Tang and Vanslyke, (1987), Tang and Vanslyke, (1989)*]. Organic EL devices have many advantages in display applications due to their high brightness, large viewing angle, ease of fabrication over large area and low-cost production. Among them, the tris (8-hydroxyquinoline) aluminum (III) (Alq_3) is the most important and widely studied material.

Since the organic thin film is directly in contact with the anode material, the anode material surface properties are expected to strongly affect the characteristics of the device. A transparent conducting indium tin oxides (ITO) is widely used as anode materials of thin film OLEDs due to its good optical transparency, low electrical resistivity, ease of patterning, high work function and efficient hole injection properties [*Tang and Vanslyke, (1987), Braun and Heeger, (1991), Park et al., (1996)*]. In fabrication of OLEDs, cleaning of the ITO surface has crucial effects on the OLEDs

performance. In addition, surface states of ITO and interface properties between ITO and organic layers considerably influence the performance of OLEDs. The work function of the ITO electrode is sensitive to the surface state, and it defines the energy barrier for the hole injection from the ITO anode into the organic layer. The barrier for hole injection at the interface between the ITO anode and the organic layer has been reported to be an important factor influencing the luminescent and electrical properties of OLEDs. However, it is still not clearly understood how these treatments enhance or degrade the interface properties of ITO and OSC layer. In order to address this problem, various methods to suitably modify the surface of ITO to produce the desired electronic properties of devices have been developed. When used without surface treatments of ITO, devices usually exhibit poor device performance. Surface treatments such as chemical treatment [*Kim et al., (1998), Li et al., (1997), Nuesch et al., (2000)*], plasma treatment [*Furukawa et al., (1997), Wu et al., (1997), Kim et al., (1999), Chan, et al., (2001), Jeong, et al., (2006)*] and ultraviolet (UV)/ ozone (O_3) [*So et al., (1999), Mason et al., (1999), Song et al., (2001), Fukushi et al., (2005), Li et al., (2005)*] have been developed to improve the charge injection from the ITO into organic layer.

Kim et al [*Kim et al., (1998)*] studied the influence of aqua regia treatment and combined oxygen (O_2) plasma and aqua regia in different order. They recommended O_2 plasma treatment alone as the best treatment in their study. Li et al [*Li et al., (1997)*] observed improvements in the device performance with aqua regia treatment in their study where the improvements of hole injection is due to increased surface roughness as a result of acid treatment. This contradicts with the results reported by Kim et al [*Kim et al., (1998)*]. Nuesch et al [*Nuesch et al., (2000)*] studied O_2 plasma treatment prior to

acid treatment and they reported that the device performance was improved as a result of the increase in work function attributed by the protonation of the ITO surface and the formation of surface dipoles.

Furukawa et al [*Furukawa et al., (1997)*] studied the effects of using different gases in the plasma treatments of the ITO surface on the performance of EL devices. They reported that argon (Ar) plasma treatment and air plasma treatment were effective in the removal of contamination from the ITO surface thus improving the EL properties. Wu et al [*Wu et al., (1997)*] reported that the O_2 plasma treatment was most effective in preparing the ITO surface for high performance OLEDs and the Ar plasma treatment produced only a slight improvement to the device due to the surface cleaning effect of Ar plasma. Chan et al [*Chan, et al., (2001)*] reported that atmospheric plasma treatment of the ITO surface was more efficient compared to the above treatments in enhancing the OLED device characteristics. They attributed this to the increase in the work function of ITO and reduction in the carbon contamination of the ITO surface, thus enhancing the hole injection. In the study by Jeong et al [*Jeong, et al., (2006)*], among the various gases plasma treatments on ITO substrates; they found that fluorocarbon (CF_4) plasma treatment of the ITO surface showed the best OLED device characteristics and was believed to be due to higher increase in the work function of ITO and decrease in the hole injection barrier by the thin CF_x buffer layer formed on the ITO surface. Methane (CH_4) plasma treatment of the ITO surface resulted in the worst OLED device characteristics was related to the formation of a hydrocarbon (C:H) layer on the ITO surface. OLEDs fabricated from UV/O_3 treated ITO substrates were reported to have a low turn-on voltage and better brightness as this treatment was effectiveness in

removing organic contamination on the ITO surface by So et al [*So et al., (1999)*]. Mason et al [*Mason et al., (1999)*] reported that the improvement in the device performance of OLED with the ITO surface treated by UV/O$_3$ was due to the increase in the surface oxygen concentration and work function. Song et al [*Song et al., (2001)*] reported that most of the carbon contamination at the ITO surface was removed by UV/O$_3$ treatment. They also found that UV/O$_3$ treatment introduced O^{2-} ions onto the ITO surface and decreased the carrier concentration at ITO surface, thus decreased the conductivity of ITO surface. Fukushi et al [*Fukushi et al., (2005)*] reported that UV irradiation was effective in varying the surface roughness of the ITO surface thus achieving longer OLED lifetime due to the removal of the organic contaminants on the ITO surface.

OLEDs using crystal silicon (c-Si) as the anode material have also been studied for applications in silicon electronics and light emitting devices [*Ran et al., (2005), Ma et al., (2006)*]. Applications also include interlayer dielectric in plastic substrate field-effect transistor (FET) devices, organic thin film transistors (OTFTs) and passivation layers for elemental and compound semiconductor device structures. However, the light emitting efficiency of the EL device fabricated on c-Si was very low and not suitable for light emitting application. The OLEDs with p-type c-Si anodes demonstrated low performance, with the highest brightness of only 100 cd/m^2 at 15 V [*Parker and Kim, (1999)*]. Zhou et al [*Zhou et al., (1999)*] used a p-type c-Si as the anode to fabricate OLEDs instead of the ITO. They found that the c-Si anode resulted in an increase in hole injection in the OLED compared to the OLED with ITO anode.

The first step in the fabrication of semiconductor devices using c-Si as the substrates is the preparation of a smooth surface almost free of native-oxides and defects. Aqueous HF solution has been widely used in cleaning c-Si surfaces producing stable, hydrogen-terminated surfaces [*Takahagi et al., (1988), Dumas and Chabal, (1991), Houston and Maboudian, (1995)*]. The hydrogen-terminated silicon surface is reported to be hydrophobic and prevents oxidation when exposed to air ambient. Levenets et al [*Levenets et al., (1995)*] reported that silicon surface treatment with aqueous HBF_4 solution resulted in removal of the silicon native oxide and leaving behind a silicon surface covered with hydrogen and fluorine atoms. Another fluorine-based chemical such as NH_4BF_4 [*Kawabata and Adachi, (1999)*] and H_2SiF_6 [*Tomita et al., (2000)*] aqueous solutions have been reported to attack the silicon native oxide leaving behind a shiny flat surface. It has been reported that an aqueous solution of NaF causes the removal of the native oxide on Si (111) upon immersing the sample into the solution [*Finne and Kline, (1967)*].

Ramm et al [*Ramm et al., (1991), Ramm et al., (1994)*] showed that a low energy (discharge voltages smaller than 30 V) direct current (DC) plasma process, called plasma chemical cleaning, can be used to clean the native oxide and carbon contamination from the silicon surface without any pretreatment on the wafers. Kafader et al [*Kafader et al., (1995)*] also reported that the native oxide and carbon contamination on silicon wafers can be removed *in situ* by a DC H/Ar-plasma cleaning process and emphasized the fact that no pre-treatment of the wafers was necessary.

Different hydrogen-plasma etching facilities, using electron cyclotron resonance (ECR) [*Diani et al., (1992)*] or radio frequency (RF) [*Anthony et al., (1989)*] plasma,

have been developed for cleaning the silicon substrates. Donose et al [*Donose et al., (2006)*] reported that the silicon oxide layers from the silicon wafers were cleaned by water-vapor plasma cleaning combined with UV/O$_3$. The removal of organic contaminants present on the surface of silicon wafers by dry cleaning method using UV/O$_3$ and ECR plasma were also reported by Choi et al [*Choi, (2003)*].

It is obvious that surface treatment techniques done on the substrates used in organic semiconductor thin film devices as discussed above is very crucial in the performance of the devices. Plasma treatment using various gases and UV/O$_3$ treatment are among the most widely investigated techniques and have been proven to be effective in removing organic contaminants and increasing the work function of the substrate material thus enhancing hole injection. These properties are very important in obtaining high performance organic semiconductor thin film devices when these substrates are used as the anode material. Plasma discharge of reactive gases produces radicals forming a layer of film on the substrates or inserting atoms into the material structure and energetic ions bombarding the surface of the substrates. UV/O$_3$ treatment involves absorption of UV photon energy by weak bonds at the surface resulting in broken bonds and insertion of O atoms at the surface of the film structure. This has a significant effect on the property of the substrate material at the surface.

In this work, Alq$_3$ films are deposited on ITO and p-type c-Si substrates. The ITO and c-Si substrates are cleaned using normal wet chemical treatments with acetone to remove grease and other organic contaminants followed by ultrasonic bath rinse in deionized water. The ITO substrates are etched in concentrated hydrochloric acid (HCl) solution to remove oxide contaminants until the required resistivity is acquired while

the c-Si substrates are etched in hydrogen fluoride (HF) solution to remove oxides on the c-Si surface. Five sets of Alq_3 films on ITO and p-type c-Si substrates are studied in this work consisting of films deposited on these substrates exposed to different time duration of methane (CH_4), helium (He), argon (Ar), oxygen (O_2) plasma, and UV/ozone (UV/O_3) treatment. Photoluminescence (PL) and electrical properties of these Alq_3 films on these substrates are studied. The PL emission intensity and peak position of each film are determined. The threshold voltages (V_T), threshold current (J_T), OLED driving voltages (V_d) and the Fowler-Nordheim (FN) plots are obtained from the current-voltage measurements done on the ITO/Alq_3/Al and c-Si/Alq_3/Al heterostructures using the untreated and treated ITO and c-Si as the anode material. From the FN plots, the hole injection barrier (Φ_h) characteristic of each of the films is calculated.

The motivation of this work is mainly to satisfy three important objectives as listed below:

- to study the effects of CH_4, He, Ar, O_2 plasma, and UV/O_3 treatment time on the PL properties of Alq_3 films deposited on ITO and p-type c-Si substrates.

- to study the effects of CH_4, He, Ar, O_2 plasma, and UV/O_3 treatment time on the electrical properties of Alq_3 films deposited on ITO and p-type c-Si substrates.

- to study, analyze and compare the PL and electrical properties of Alq_3 films deposited on ITO and p-type c-Si substrates.

- to design and build a thermal evaporation system for Alq_3 thin film deposition.

This thesis consists of five chapters. Chapter 2 contains the literature review on organic semiconductor which includes OLED and its device structure. A brief review on

Alq$_3$ is also included. The principles of the OLEDs operation and the surface treatments on the anode material are also discussed. The final part of this chapter reviews the various characterization techniques used in studying vacuum evaporated Alq$_3$ film.

Chapter 3 presents the experimental techniques involving sample preparation, surface treatment techniques and characterization technique of Alq$_3$ films on ITO and c-Si substrates. The chapter ends with descriptions on the photoluminescence spectroscopy and current-voltage measurements techniques used in this work.

The results and discussions on the results obtained in this work are presented in Chapter 4. This chapter is divided into two main sections. The first section discusses the photoluminescence properties while the second section discusses the electrical properties of the Alq$_3$ films on ITO and p-type c-Si substrates. The effects of the various surface treatments done on the anode material on the photoluminescence and electrical properties of the films are discussed in this chapter.

Chapter 5 concludes the results obtained from this work along with suggestions for future works.

Chapter 2 Literature Review

2.1 Organic Semiconductor

2.1.1 Introduction

At the beginning of the 21st century, we are facing a new electronics revolution fueled by the drastic development and understanding of a new class of materials, commonly known as Organic Semiconductors (OSCs). Although organic semiconducting materials have been synthesized and studied for many years particularly in the 1950s, previously the performance and stability of organic semiconducting materials were poor [*Gutmann and Lyons, (1967)*]. Nevertheless, with strong improvements in synthesis and processing of new classes of molecules, the potential of using OSCs in applications such as organic light-emitting diodes (OLEDs), field-effect transistors (OFETs) and the solar cells is now greater than ever. The lower costs and simplicity in manufacturing these organic devices are the primary reasons for the drive towards commercialization.

2.1.2 Materials

Basically, there are two major classes of OSCs: low molecular weight materials and polymers. Both have in common, a conjugated π-electron system being formed by the p$_z$-orbitals of sp^2-hybridized C-atoms in the molecules (see Fig. 2.1). Carbon p$_z$-orbital overlapped and the π-electron become delocalized on the molecule, forming the so called π-conjugated system [*Dimitrakopoulos and Mascaro, (2001)*]. The alternating single and double bonds in polymer drawings represent these π-electron. As compared to the σ-bonds which forms the backbone of the molecules, the π-bonding is

significantly weaker. Therefore, the lowest electronic excitations of conjugated molecules are the π-π*-transitions with an energy gap typically between 1.5 and 3 eV leading to light absorption or emission in the visible spectral range. Fig. 2.2 shows some important OSCs such as pentance, phthalocyanines, and etc., which demonstrated good semiconducting properties.
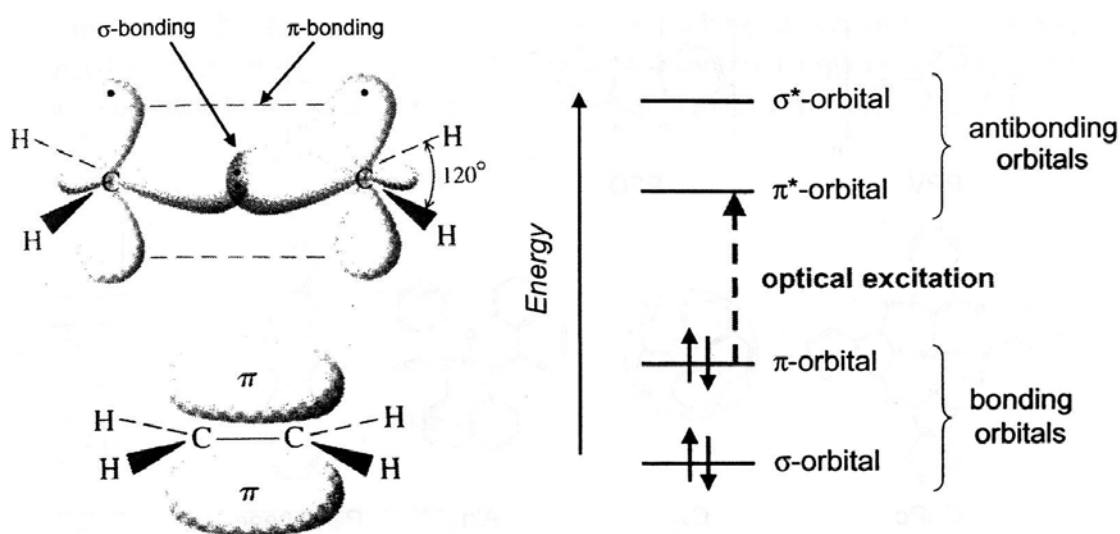
Fig. 2.1. Left: σ- and π-bonds in ethane, as an example for the simplest conjugated π-electron system. The right viewgraph shows the energy levels of a π-conjugated molecule. The lowest electronic excitation is between the bonding π-orbital and the antibonding π*-orbital [*Brutting, (2005)*].

Pentacene has been studied intensely for research on organic thin film transistors and OFETs. Pentacene is one of the most thoroughly investigated conjugated organic molecules with a high application due to a hole mobility in OFETs which exceeds that of amorphous silicon [*Pan and Sun, (2009), Datta and Kumar, (2010)*].

The major application of rubrene as an organic semiconductor is in OLEDs and OFETs. Single-crystal transistors can be prepared using crystalline rubrene. Rubrene holds the distinction of being organic semiconductor with the highest carrier mobility for holes [*Choi et al., (2009), Liu et al., (2010)*].
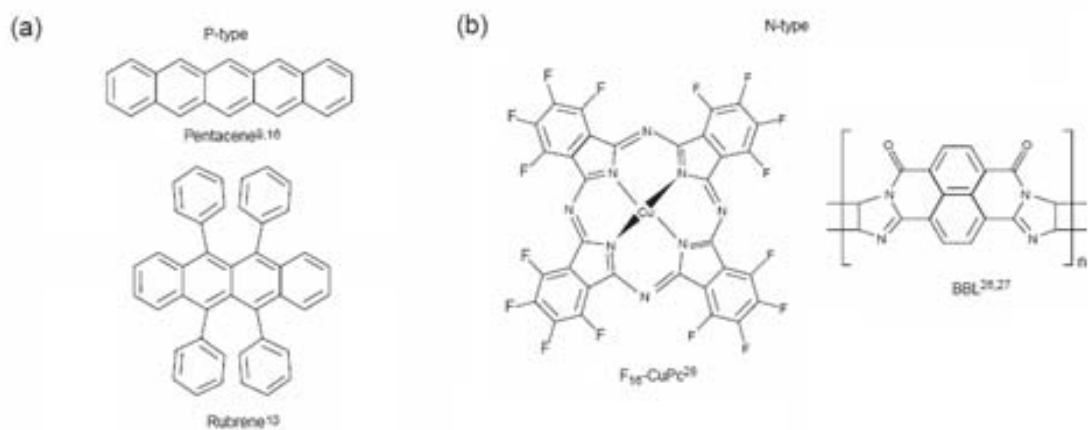
Fig. 2.2. Prominent (a) p- and (b) n-type organic semiconductor materials [*Laudise et al., (1998), Yeates et al., (2001), Brutting, (2005)*].

Phthalocyanines ($F_{16}CuPc$) exhibit certain degree of specific tenability, due to possible central metal ion, which can be changed within a broad range, and due to the choice of the sidegroup. $F_{16}CuPc$ is considered a good candidate as an n-type conducting material, and also as a blue dye, it is interesting for optoelectronic applications [*Bao et al., (1998), Rogers et al., (2000), Alonso et al., (2003)*].

Poly-benzimidazobenophenanthroline (BBL) is a fully conjugated ladder polymer first synthesized as a structural material for its anticipated high tensile strength. BBL has being one of the interest candidates as a conductive and nonlinear optical material due to its electronic conjugation. For example, pristine BBL is a semiconductor with a room temperature [*Dalton et al., (1987), Coter et al., (1989), Yeates et al., (2001)*].

An important conjugated low-molecular weight organic material (small molecules), which is the material of choice for all the experiments and analysis presented in this work, is the Tris (8-hydroxyquinoline) aluminum (III) (Alq_3). Fig. 2.3 shows a sketch of this molecule. The interest in Alq_3 as the active layer in organic light-emitting devices (OLED) started with a report on the efficient electroluminescent devices produced using

Alq$_3$ as an electron-transport layer and light emitting layer in the 1980s. [*Kumar et al., (2005), Tang and Vanslyke, (1987)*]. Alq$_3$ is a stable metal chelate that can be deposited as thin films by using vacuum deposition method and stands as one of the most successful materials used in organic electroluminescence applications. These OLEDs opened the way for a new generation of flat panel displays.
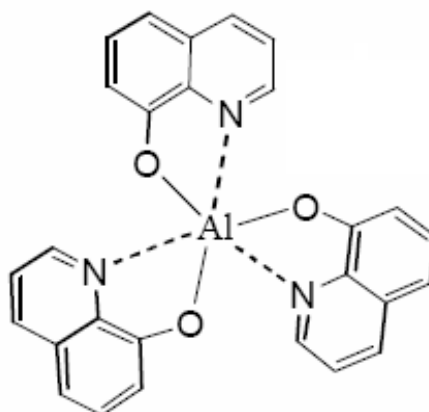
Fig. 2.3. Chemical structure of Tris (8-hydroxyquinoline) aluminum (III) (Alq$_3$).

Even after nearly two decades of intensive research and development of OLEDs, Alq$_3$ still continues to be the workhorse in low-molecular weight materials for these devices. It also serves as host material for various dyes to tune the emission colour from green to red [*Tang and Vanslyke, (1989)*]. The OLEDs produced shows excellent stability and luminescent properties and exhibits many advantages over inorganic LEDs. They also requires low operating voltages and low power consumption.

Most studies to date are concentrated on the optimization of the device characteristics [*McElvain et al., (1996)*], improvement of the morphological stability [*Do et al., (1996)*], understanding the mechanism of charge transport and the specifics of EL of Alq$_3$ based OLEDs [*Burrows and Forrest, (1993)*]. However, Alq$_3$ is usually

susceptible to environment aging and photo-oxidation, which influences their viability for commercial usefulness [*Priestley et al., (2002)*]. Short lifetime, low carrier mobility and high interface barriers must be improved by optimizing the material parameters and fabrication steps.

2.2 Organic Light-Emitting Diodes

2.2.1 Structures of OLEDs

The simplest OLED configuration consists of a single organic layer sandwiched between the anode and the cathode, as shown in Fig. 2.4. When a voltage is applied or a current exists in the device such that the anode is positive with respect to the cathode, this causes a current of electrons to flow through the device from cathode to anode. The electrons and the holes move towards each other and recombine while the emissive layer becomes negatively charged, and the conductive layer becomes positively charged holes. The recombination causes a drop in the energy levels of electrons, accompanied by an emission of radiation whose frequency is in the visible region (visible light emission). That is why this layer is called emissive layer.
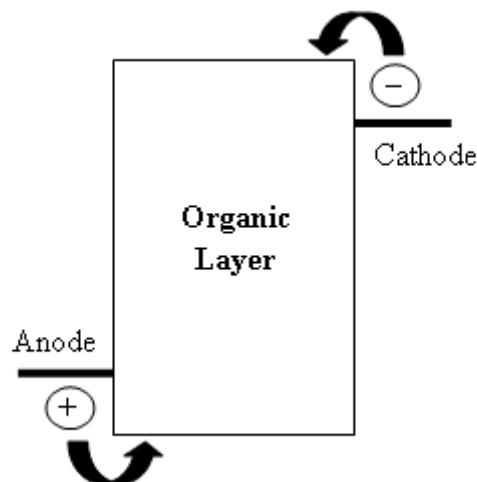
Fig. 2.4. The energy level diagram of single layer OLED devices.

The anode has to be a conducting material and also transparent in order to allow the light emit throughout of the device. The anode has to be chosen from high work function material where its work function is within the range of 4.7 – 4.9 eV because it is closer to the Highest Occupied Molecular Orbital (HOMO) of the organic material. Indium tin oxide (ITO) is commonly used as the anode material. It is transparent to visible light and has a high work function of 4.8 eV [*Park et al., (1996)*] which promotes injection of holes into the organic layer. Meanwhile, the cathode has to be chosen from low work function metal where its work function is closer to the Lowest Unoccupied Molecular Orbital (LUMO) of the organic material. Metals such as aluminum and calcium are often used for the cathode as they have low work functions which promote injection of electrons into the organic layer.

2.2.2 Mechanisms of Charge Injection and Transport in Organic Semiconductors

The performance of the OLEDs critically depends on the nature of charge injection from the contacting electrodes into the OSC, followed by the effective transport of the carriers through the bulk of the material. In LEDs [*Shaw and Seidler, (2001)*], the effective injection of the holes and electrons from the contacts is followed by transport through the bulk, leading to recombination and emission of light.

2.3 Principles of OLED Operation
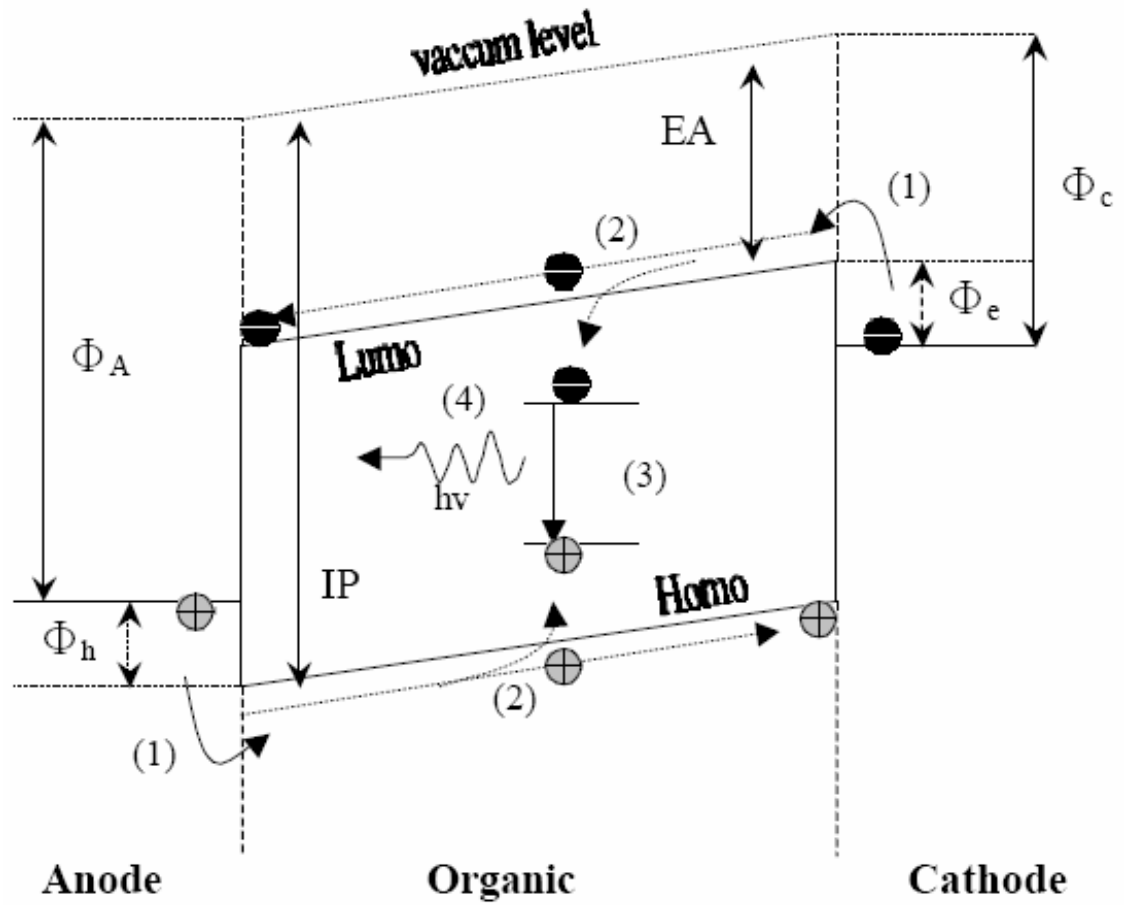
Fig. 2.5. Structure and schematic energy level diagram of a single layer OLED, Φ_A: anode work function, Φ_C: cathode work function, Φ_h: hole injection barrier, Φ_e: electron injection barrier, IP: ionization potential, EA: electron affinity. The basic steps of EL: (1) charge carrier injection, (2) charge carrier transport, (3) exciton formation, and (4) radiative exciton decay [*Hadziioannou and Hutten, (2000)*].

The operation of OLED involves several steps including the injection, transport, capture and radiative recombination of positive and negative charge carriers inside an organic layer with a suitable energy gap to emit visible light. Fig 2.5 illustrates the schematic operation steps of the spatial variation of the molecular energy levels in a band-like fashion. These steps are described below:

2.3.1 Charge Injection and Charge Transport

The holes are injected from the anode to the HOMO or valence band (π) while the electrons are injected from the cathode to the LUMO or conduction band (π^*) by the influence of electric field. The injected electrons and holes transport through the organic layer in the applied field. Thus, the cathode gives electrons to the emissive layer and the anode withdraws electrons from the conductive layer. Injection of charges from most electrode materials requires that charges tunnel through barriers at the interface. The size of energy barriers between electrodes and the organic layers usually scales with the electrodes work functions, which are important in determining device performance.

Fig. 2.6 (a) illustrates the energy-band diagram of OLED devices when the device under zero applied bias, where no currents exist and no external excitation is applied. Injection of charge to the organic layer is not occurred when zero applied bias. However, flat band condition occurs when voltage applied is equilibrium to the difference between the work function of anode and cathode as shown in Fig 2.6 (b) [*Chiguvare et al., (2003)*]. This is the minimum voltage yield for electrons and holes injection process to occur.
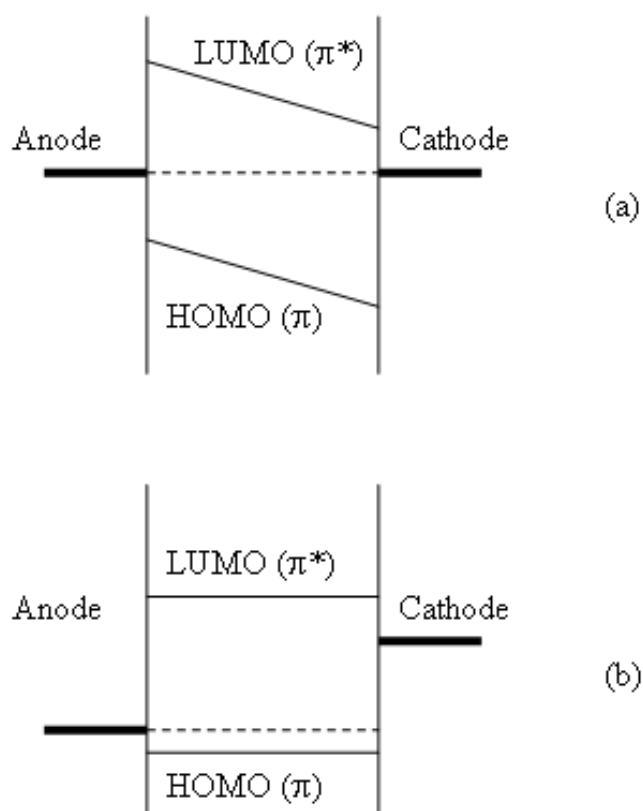
Fig. 2.6. Electronic structures for an OLED in (a) zero biased condition and (b) flat band condition.

2.3.2 Electron-hole Recombination and Exciton Formations

After the charges are injected into the organic layer, under the influence of the electric field the electrons and holes will move towards each other and recombine at the recombination zone; cause an emission of light due to the drop of energy levels of the electrons. The process of electron-hole confinement in the OLEDs is an important aspect to the device operation. It is necessary for one or the other low mobility charge carriers to get efficiently confined in these very thin structure (with the thickness of the organic at approximately ~ 1000 Å), such that the local charge density is sufficiently high to ensure the other charge carrier will pass within a confined radius of at least one charge. After the electron-hole confinement process, excitons are formed. The total spin

of excitons generated by carrier recombination can be at a triplet or singlet state. The triplet exciton is strongly bound with respect to the singlet where three quarter of the electron-hole pairs is expected to dissipate due to non-radiative decay of triplets. However, triplet emission can be harvested for highly efficient OLEDs [*Klaus and Ullrich, (2006)*].

2.3.3 Radiative and Non-radiative Decay of Singlet Excitons
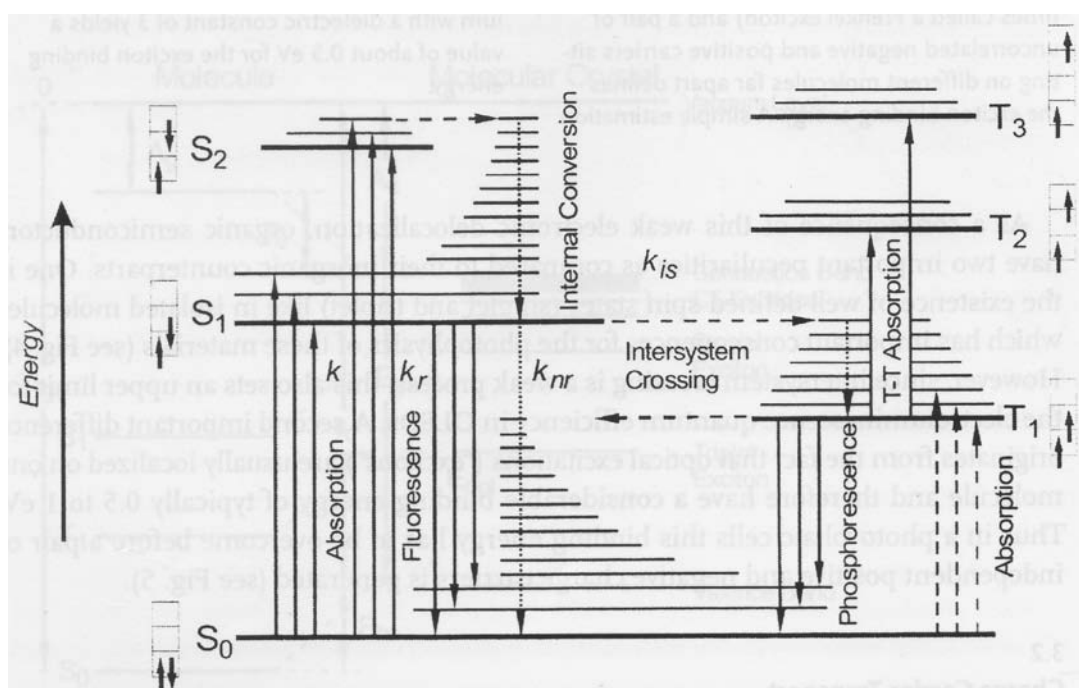
Fig. 2.7. Energy level scheme of an organic molecule (left: singlet manifold, right: triplet manifold). Arrow with solid lines indicate radiative transitions, those with broken lines indicate non-radiative transitions [*Pope and Swenberg, (1982)*].

When singlet excitons form, energy relaxation will take place through several ways. First, the singlet excitons may emit a photon of light of energy equal to the difference between the first excited state and ground state. This process is called fluorescence which is the desired radiative decay. It is also possible for non-radiative processes to occur where an electron in the excited singlet state undergoes a spin transition, leading

to the triplet excited state, or decays with thermal and quenching effects. The number of excitons generated is usually proportionate to the number of injected carriers. So the luminescence intensity also scales with current (see Fig. 2.7) [*Pope and Swenberg, (1982)*].

2.4 Surface Treatment on Anode Material

Many problems with optical and electrical device performance have been found to occur at the contact interface between the anode material and the organic layer [*Haines and Bube, (1978)*]. The physical and chemical nature of the substrate surface is complex and both morphology and surface chemistry may influence the charge injection across the anode material interface which is critical for the device performance. By modifying the surface properties of the anode material, the work function of the anode can be varied to manipulate the hole-injection energy barrier. Without surface treatment of the anode material, the OLED devices usually exhibit poor performance. Many types of surface treatments of the anode material have been employed to improve the device performance. In this work, two methods have been employed for the anode material surface treatment, which include the RF plasma using Methane (CH_4), Helium (He), Argon (Ar), Oxygen (O_2), and by Ultraviolet/ozone (UV/O_3) surface treatment.

2.4.1 Radio Frequency Plasma Surface Treatment

RF plasma surface treatment employs the active species produced in a plasma to modify the surface characteristics of the solids or thin films. Plasma surface treatment may add or remove adsorbed monolayers or induces chemical reactions with the surface. The treatment may also add or remove surface charge and it may change the physical or chemical state of the superficial monolayers of a material.

This treatment may be classified by the surface property altered. These surface property effects may include: decontamination and sterilization that increases the surface energy and alters the electrical characteristics or surface finishing of a material; chemically grafting the functional group on the surface to achieve improved surface characteristics (plasma cleaning) [*Wu et al., (1997)*]. The contaminants may take the form of adherent monolayers of hydrocarbons, thin layer of chemical reaction products of the surface material (e.g. oxides), or layer of contaminants (dirts). Plasma may also damage or altered the bulk material, induce changes on the chemical state of the bulk material below the surface (plasma etching) [*Purvis et al., (2000), Park et al., (1996)*], and add monolayers onto the material surface (plasma deposition) [*Jeong et al., (2007)*].

2.4.2 UV/ozone Surface Treatment

Ultraviolet (UV) and ozone (O_3) (UV irradiation with O_2 flow) cleaning method has been applied to various kinds of semiconductors such as Si [*Krusor et al., (1986) and Suemitsu et al., (1989)*] and is a viable technique for removing hydrocarbon contamination on the ITO surface [*So et al., (1999)*], creation of surface dipoles, change in ration of surface constituents (Sn, In, O) and Fermi shift [*Yu et al., (2001)*] and

reducing the interface defects which means that the initial surface conditions before oxidation, such as surface contaminations, surface morphology [*Fukushi et al., (2005)*], affect the interfacial characteristics [*Kosugi et al., (2000)*]. UV irradiation allows cutting the quantity of molecular bonding of organic contaminants and the released molecules react with the excited oxygen atoms with a high oxidation power forming gases such as CO_2 and H_2O, and removal of organic contaminants and make the surface clean [*Iso et al., (1999)*]

2.5 Current-Voltage Analysis

The current-voltage (*I-V*) characteristic as shown in Fig. 2.8, is the main indicator in determining the rectifying property such as threshold voltage (V_T), threshold current (J_T) and OLED driving voltage (V_d) for fabricated OLEDs. The OLED device that shows this rectifying property would be able to produce light emission. An ideal rectifying device operates in a forward biased condition where the electric current flow will increase with the increasing in applied voltage. When the device is in reverse biased condition, only small electric current is conducted with the increase in voltage.
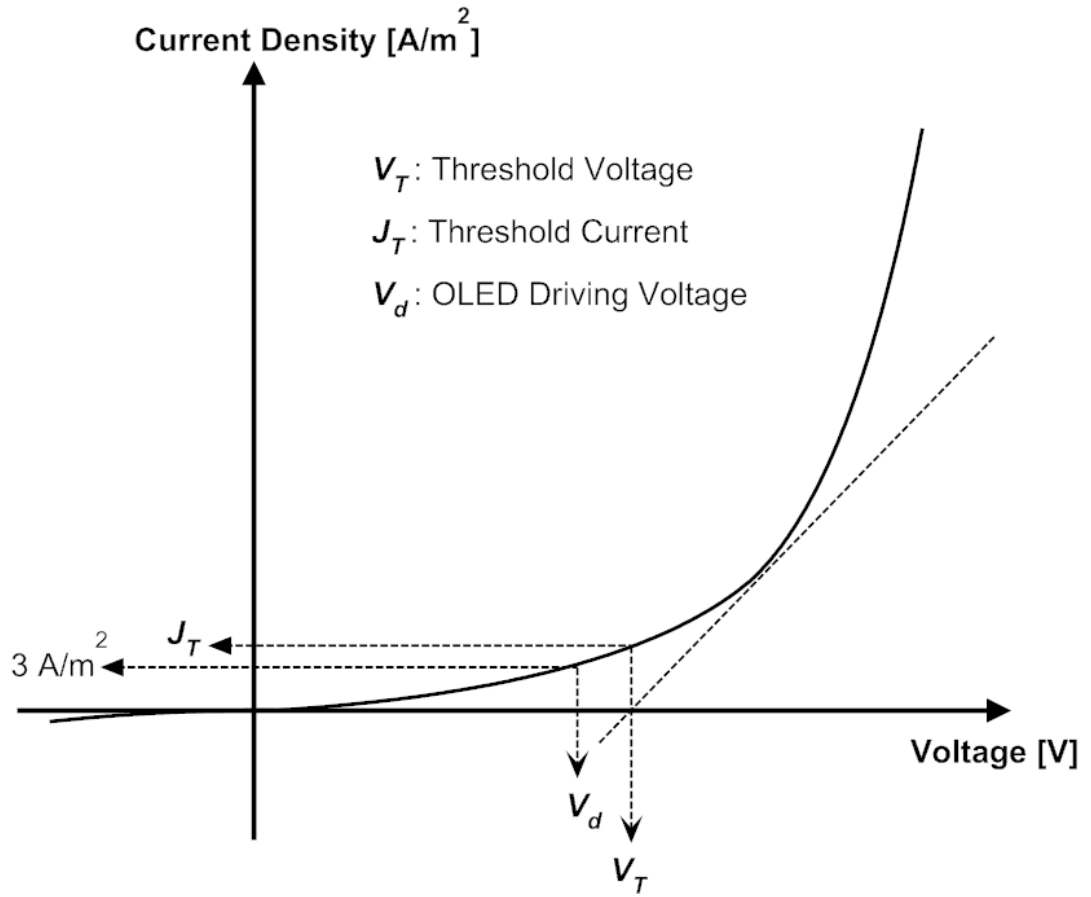
Fig. 2.8. Current-voltage characteristic of rectifying diode.

The V_T marks the sudden increase in current with increase in voltage applied in the forward bias (positive [+] at ITO and [-] at Al) [*Klaus and Ullrich, 2006*]. The device current density, j_T is the sum of the injected electron current density, j_e and the hole current density reaching the cathode , j_h' without recombination or the sum of the injected hole current density, j_h and the electron current density reaching the anode, j_e' without recombination.

$$j_T = j_e' + j_h = j_e + j_h' \tag{2.1}$$

$$j_e = ne\mu_e \quad \text{and} \quad j_h = pe\mu_h \tag{2.2}$$

$$j_e' = n'e\mu \quad \text{and} \quad j_h' = p'e\mu_h \tag{2.3}$$

where n, p, n', p' e, μ_e, and μ_h are number of injected electrons and holes, number of

electrons and holes reaching the counter electrodes without recombination, electronic charge, mobility of electrons and holes respectively.

In this work, no change in electron injection is expected as the surface treatment is done on the anode material surface. Therefore, the changes observed are expected to be due to j_e' and j_h. In Alq$_3$ films, electron mobility is about two magnitudes higher than hole mobility [*Li and Meng, (2006)*]. When electrons and holes are injected into Alq$_3$ from the cathode and anode respectively, they would meet in the region close to the anode. Accumulation of electrons at the anode/Alq$_3$ interface would form an electron abundant layer at the interface if leakage current, j_e' is small and local electric field effect would favour hole injection into Alq$_3$, enhancing j_h. Usually, hole injection is enhanced as a result of formation of a dipole layer at the anode/Alq$_3$ interface as this has been reported to lower electron or hole injection barrier [*Xu et al., (2007)*]. The presence of electron/hole traps levels due to defects and impurities at the anode surface or in the Alq$_3$ film has the adverse effect of reducing the number of electrons at the interface thus reducing j_h and j_e'.

The number of conduction electrons and holes are determined by electron injection barrier at the Alq$_3$/Al interface, Φ_e and hole injection barrier at the ITO/Alq$_3$ interface, Φ_h respectively.

$$\Phi_e = \Phi_{Al} - \chi_{Alq_3} - \delta_{Al/Alq_3} \tag{2.4}$$

$$\Phi_h = \Phi_{ITO} - \chi_{Alq_3} - \delta_{ITO/Alq_3} \tag{2.5}$$

The electron affinity of Alq$_3$, χ_{Alq_3} is the energy difference between the vacuum level and Fermi level of Alq$_3$. The energy band diagram of the ITO/Alq$_3$/Al and c-Si/Alq$_3$/Al heterostructure is shown in Fig. 2.9.
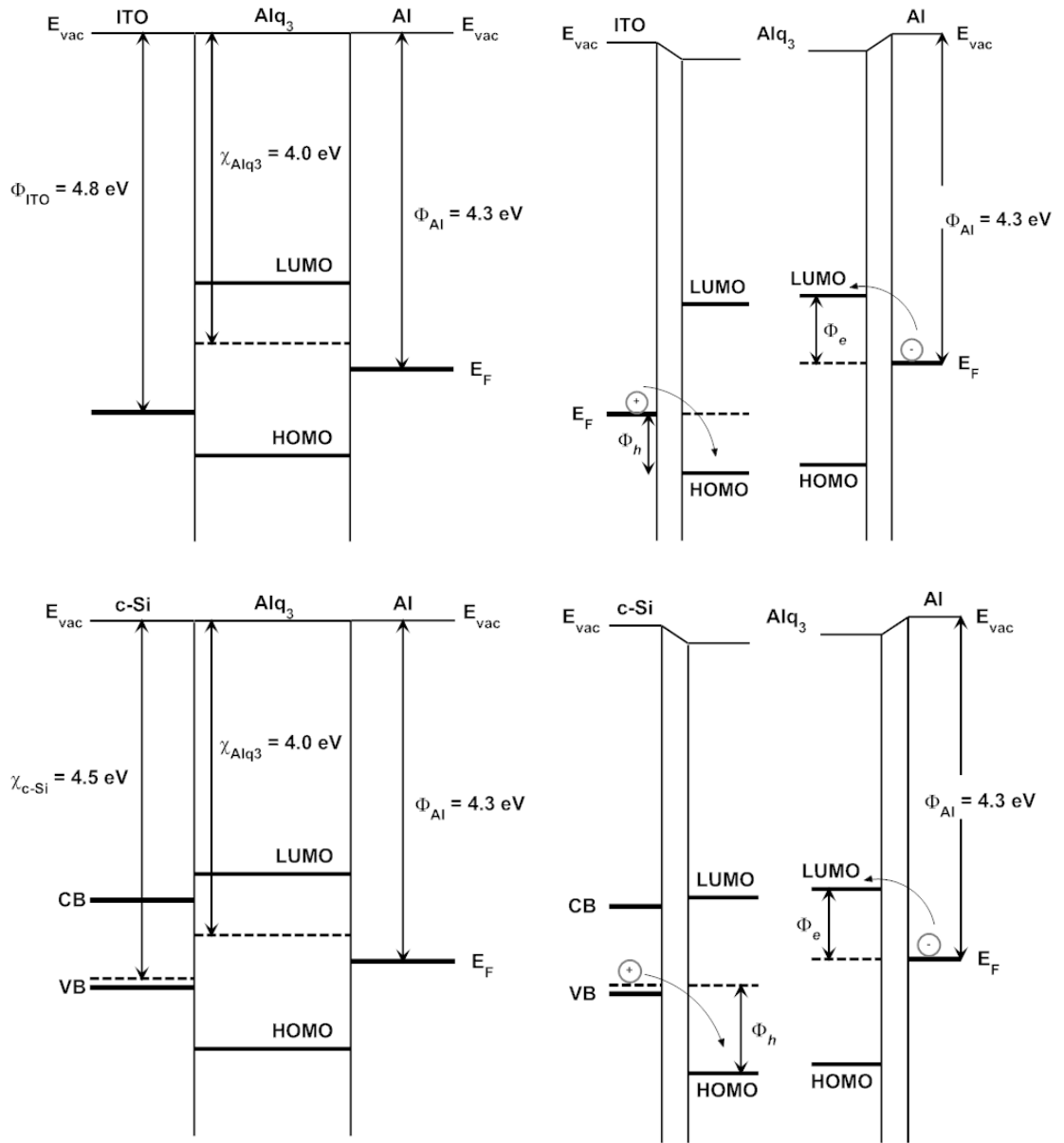
Fig. 2.9. Energy band diagram of ITO/Alq$_3$/Al and c-Si/Alq$_3$/Al heterostructure.

To further analyze the *I-V* measurement, the Fowler Nordheim (FN) model is adopted in order to estimate the barrier height at the interface, Φ_B. The theory assumes that current is limited solely by high injection barriers which imply that no space charges are present and therefore the electric field present is homogeneous. The FN tunneling is the flow of electrons through a triangular potential barrier [*Schroder, (1998)*]. The FN current I_{FN} is given by the expression

$$I_{FN} = AK_1 E^2 \exp\left(\frac{-K_2}{E}\right) \tag{2.6}$$

where A is the area, E is the electric field, and K_1 and K_2 are usually considered to be constants. Rearranging the Eq. (2.6) gives

$$\ln\left(\frac{I_{FN}}{AE^2}\right) = \ln\left(\frac{J_{FN}}{E^2}\right) = \ln(K_1) - \frac{K_2}{E} \tag{2.7}$$

K_1 and K_2 are given by

$$K_1 = \frac{q^3 m^*}{8\pi h \Phi_B} \tag{2.8}$$

$$K_2 = \frac{8\pi\sqrt{2m^* \Phi_B^3}}{3qh} \tag{2.9}$$

where Φ_B is the barrier height, m^* is the effective mass of the carriers, q is the electronic charge, and h is the Planck's constant.

A plot of $\ln (J_{FN}/E^2)$ versus $1/E$ is known as a FN plot, should be a straight line if the conduction through the organic layer is pure FN conduction. The intercept of this linear FN plot gives K_1 and the slope yields K_2. FN plots require knowledge of current density and electric field. What is measured is the current as a function of voltage. The current density is simply the measured current divided by the electrode area. With E in units of V/m, the electric field is given by

$$E = \frac{V}{d} \tag{2.10}$$

where V is the applied voltage and d is the thickness.

From the FN plot, if we assume that the injected charge is tunneling through a triangular energy barrier at the organic-electrode interface [*Parker, (1994)*], the barrier height Φ_B can be determined by calculating the slope K_2 of the straight line using the of Eq. (2.9), by assuming m^* is equals to the free electron mass [*Sze, (1981)*].

Chapter 3 Experimental Method

3.1 Introduction

In this chapter, the experimental and measurement techniques that were done on the Alq$_3$ thin films will be discussed in detail. Firstly, the substrate preparation which include the substrate cleaning procedure and anode preparation used for Alq$_3$ film deposition will be presented. Prior to the organic layer (Alq$_3$) deposition, the procedure of surface treatment on anode material will be discussed in the next section and followed by the fabrication of the Alq$_3$ film. The final section presents the characterization techniques which include the Photoluminescence (PL) Spectroscopy and current-voltage (*I-V*) measurement to obtain the photoluminescence and electrical properties of the film.

3.2 Substrate Preparation

Thin films cannot support themselves, and thus a substrate should be used. In this work, the substrates used to deposit the Alq$_3$ films were (111) p-type crystal silicon (c-Si) wafer bought from Shinetsu Malaysia with resistivity of 1 - 10 Ωcm and Indium Tin Oxide (ITO) substrates with resistivity of 20 Ωcm. They were cut to size approximately: 2×2.5 cm^2.

3.2.1 Substrate Cleaning Procedure

The cleaning process is very important in determining the nature of the films formed. A thoroughly cleaned substrate is a precondition for the preparation of film. The choice of cleaning techniques depends on the nature of the substrate, the type of

contaminants, and the degree of cleanliness required. Residues from manufacturing and packaging, lint, fingerprints, oil, and airborne particle matter are examples of frequently encountered contaminants.

3.2.2 Anode Preparation
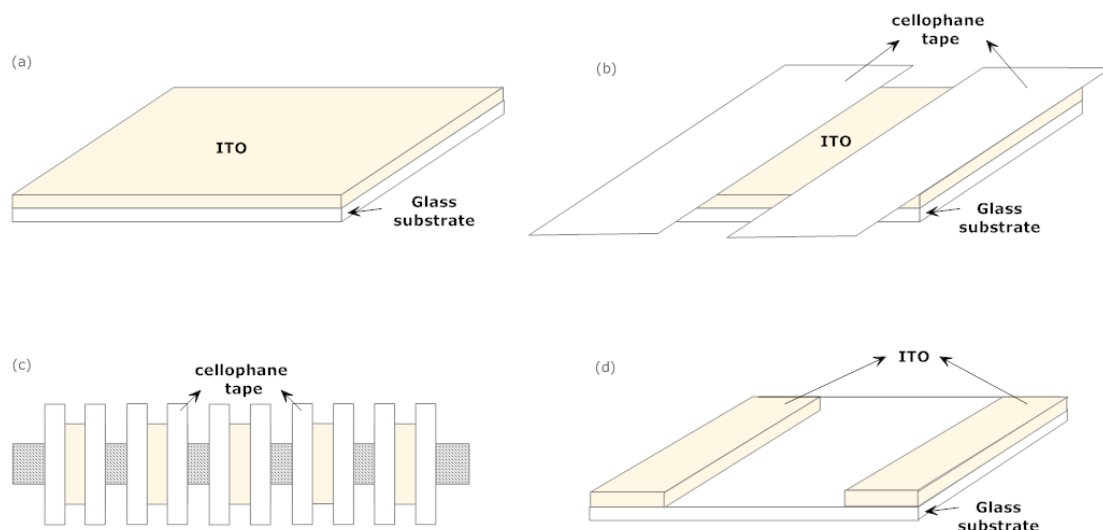
Fig. 3.1. ITO substrates patterning prior to the organic layer deposition.

Fig. 3.1 (a) showed the ITO substrates before etching. The ITO substrates with sheet resistance about $2 \times 10^{-3} \ \Omega \ cm^{-2}$ were used as anode. The ITO substrates were first etched by vapour of concentrated HCl solution to the required pattern. The etching processes were described as follows.

The ITO substrates with size of $2 \times 2.5 \ cm^2$ were pasted with cellophane tape both side at the edge of the substrates as shown in Fig. 3.1 (b). The ITO substrates were arranged along another cellophane tape as shown in Fig. 3.1 (c), then pasted on top of the beaker containing concentrated HCl solution of H_2O:HCl = 8:2 and let the etching process last about 5 minutes. The exposed ITO surface will be etched away by the vapour of concentrated HCl solution. Multimeter is used to confirm whether the entire

expose ITO surface has been etched away. If not, repeat the etching process again. Once the etching process is done, removed the cellophane tape and the etched ITO substrates were shown in Fig. 3.1 (d).

Prior to the Alq$_3$ film deposition, the ITO substrates were thoroughly cleaned with ethanol followed by acetone and then distilled water in an ultrasonic bath. Subsequently the substrates were blow-dried using nitrogen gas.

The silicon substrates were cleaned using the wet chemical treatment process under atmospheric conditions in the following order. Firstly, the degreasing of organic contaminants is done by dipping the substrates into acetone, followed by de-ionised water in an ultrasonic bath for at least 2 minutes each. The removal of surface oxides (SiO$_2$) for hydrogen-passivation of the substrates [*Kampen et al., (2000)*] were carried out by etching in concentrated HF solution of H$_2$O: HF = 10:1 for 3 minutes. The substrates were then rinsed in de-ionized water in an ultrasonic bath for at least 2 minutes. Finally, the cleaned silicon substrates were dried by nitrogen gas blowing.

3.3 Procedure of Surface Treatment on Anode Material

The cleaned silicon and ITO substrates were then subjected to surface treatment by either RF plasma or UV/ozone before deposition of the organic layer. For the RF plasma treatment, the silicon and ITO substrates were exposed to plasmas of different gases in a parallel-plate type plasma etching reactor under identical conditions (RF power 60 Watts, operation pressure 1×10^{-2} mbar, different treatment times from 1 to 20 minutes). The summary of the plasma treatment conditions are indicated in Table 3.1.

Table 3.1

Plasma treatment conditions (13.56 MHz)

	RF Power (W)	Time (min)	Gas pressure (mbar)
CH_4 plasma	60	1, 5, 10, and 20	1×10^{-2}
He plasma	60	1, 5, 10, and 20	1×10^{-2}
Ar plasma	60	1, 5, 10, and 20	1×10^{-2}
O_2 plasma	60	1, 5, 10, and 20	1×10^{-2}

The UV/ozone treatment was carried out by exposing the silicon and ITO substrates to UV irradiation source at wavelength 254 nm, supplied by an Oriel 6035 Model deuterium lamp in an enclosed housing. Based on the measured spectrum of the lamp, the silicon and ITO substrates is estimated to have been exposed to approximately 12 mW cm^{-2} at a distance of 4 cm from the lamp under an oxygen flow rate of 40 sccm. The UV irradiation is absorbed by oxygen, changing it to ozone and atomic oxygen by dissociation of the oxygen molecules. For each gasses the treatment duration is varied from 1 to 20 minutes. Table 3.2 summarizes the general UV/ozone treatment conditions. Untreated silicon and ITO substrates were used as reference for comparison purposes.

Table 3.2

UV/ozone treatment conditions (256 nm)

	UV irradiance (mW cm^{-2})	Distance (cm)	O_2 flow (sccm)	Time (min)
UV/ozone	12	4	40	1, 5, 10, and 20

3.4 Preparation of Alq$_3$ Films

The system used in the Alq$_3$ films preparation in this work is the home-built thermal evaporation system. The system is made up of four main components: the evaporation chamber, the pumping system, the electrical and current supply system and the control panel. Pictures of the deposition system and details on the system are presented in Appendix A.

A systematic operation is required for the operation of the thermal evaporation system to ensure the deposition process is done safely and successfully. A leakage free system is also important in ensuring there is minimum contamination in the film deposited. The deposition in this work is done in room temperature. The cross sectional view of the evaporation chamber is clearly shown in Fig. 3.2.

Firstly, the deposition chamber must be cleaned after every deposition process. This is to remove the left over deposits from the previous deposition. Sand paper is used to remove the deposits on the stainless steel surface of the evaporation chamber. The chamber is then cleaned with acetone to remove water and oil contaminants. When the chamber is cleaned, the substrates are placed on the substrates holder in the chamber and the chamber is then closed and sealed. The system is now ready for deposition.

Before switching on the rotary pump, ensure all the valves within the system are closed. The rotary pump is then turned on to evacuate the evaporation chamber to a pressure of $\sim 2 \times 10^{-2}$ mbar (roughing pressure). The turbo pump is turned on when the desired roughing pressure is reached. The system is pumped down by the turbo pump to a vacuum of $\sim 8 \times 10^{-6}$ mbar. With the shutter position is closed, the current supply is turned on slowly to 38 A until the alumina crucible boat is heated up and fixed up at $\sim$

185 °C. The system is ready for deposition when the desired temperature is reached.

When the alumina crucible boat temperature reached ~ 185 °C, the system is ready for deposition. First turn on the digital quartz crystal thickness monitor to monitor the thickness of the deposited Alq_3 film. Let the Alq_3 vaporized for ~ 5 minutes to eliminate the initial impurities of the deposition process before the shutter is opened. After that open the shutter and leave the deposition system to reach desired thickness of the deposited Alq_3 film. A 120 nm thick Alq_3 layer was then thermally deposited onto the silicon and ITO. The deposition rates were kept at ~ 0.4 Å/s. After the deposition process is completed, close the shutter, decrease the current supply slowly to 0 A and turn it off. After that let the system pumps down again to the pressure ~ 8×10^{-6} mbar to ensure no excess vaporized Alq_3 left in the evaporation chamber. Release the gas in the gas releaser and the sample is prepared to be taken out.

For the comparison of difference of silicon and ITO surface treatments, the substrates treated in different manner were placed on the same sample holder that includes the untreated substrate as well, and all the devices for different substrates were fabricated during the same deposition process. The deposition parameters as shown in Table 3.3 were maintained for all the samples to enable accurate comparison.
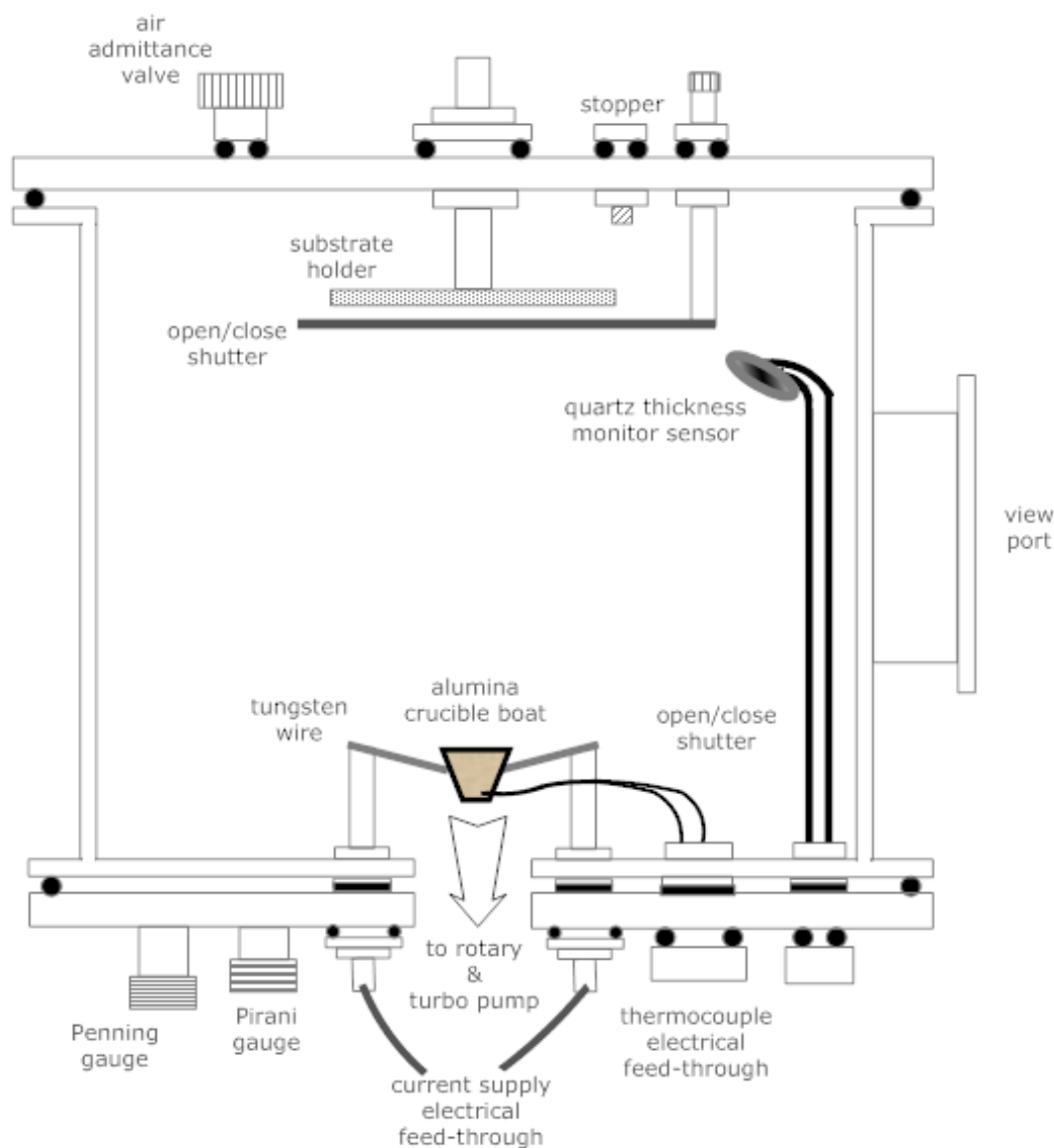
Fig. 3.2. The cross sectional view of evaporation chamber of the home-built thermal evaporation setup.

Table 3.3

Alq$_3$ organic layer deposition conditions: Substrates untreated and treated with CH$_4$, He, Ar, O$_2$ plasma, and UV/ozone for 1, 5, 10, and 20 min, respectively.

Deposition rate	Thickness	Boat Temperature	Pressure
(Å/s)	(nm)	(ºC)	(mbar)
0.4	120	180	8×10^{-6}

3.5 Characterization Techniques

3.5.3 Photoluminescence Spectroscopy

The Photoluminescence measurement were carried out on both the Alq_3 films deposited on ITO and c-Si substrates for untreated samples and those treated with CH_4, He, Ar, O_2 plasma and UV/ozone. PL spectra were recorded by using Perkin-Elmer Luminescence Spectrometer LS50B [*Perkin-Elmer Luminescence Spectrometer LS50B User Manual*]. The excitation source of the luminescence spectrometer was a Xenon flash tube coupled to a monochromator interfaced with personal computer. The PL spectra were obtained at the excitation wavelength of 224 nm.

3.5.4 Current-Voltage Measurements

Current-voltage (*I-V*) measurement is used to determine the electrical properties of Alq_3 films deposited on silicon and ITO substrates by using the Keithley 236 Source Measure Unit (SMU). Aluminium electrodes with an area of 4×3 mm^2 was deposited onto the Alq_3 surface for ITO substrates (see Fig. 3.2 (a)); while a 1 mm^2 aluminium dot was deposited onto the Alq_3 surface as the gate electrode by thermal evaporation technique. The ITO and Al layers were used as anode and cathode, respectively, in the *I-V* measurements. Aluminium layer of 400 nm thick were deposited in transverse configuration at the back of the c-Si substrates as the current injecting electrodes (see Fig. 3.2 (b)). The *I-V* measurements were measured at room temperature and were driven by a computer interface. The electrical contacts with the devices were carried out using probe tips on a Signatone Probe Station.
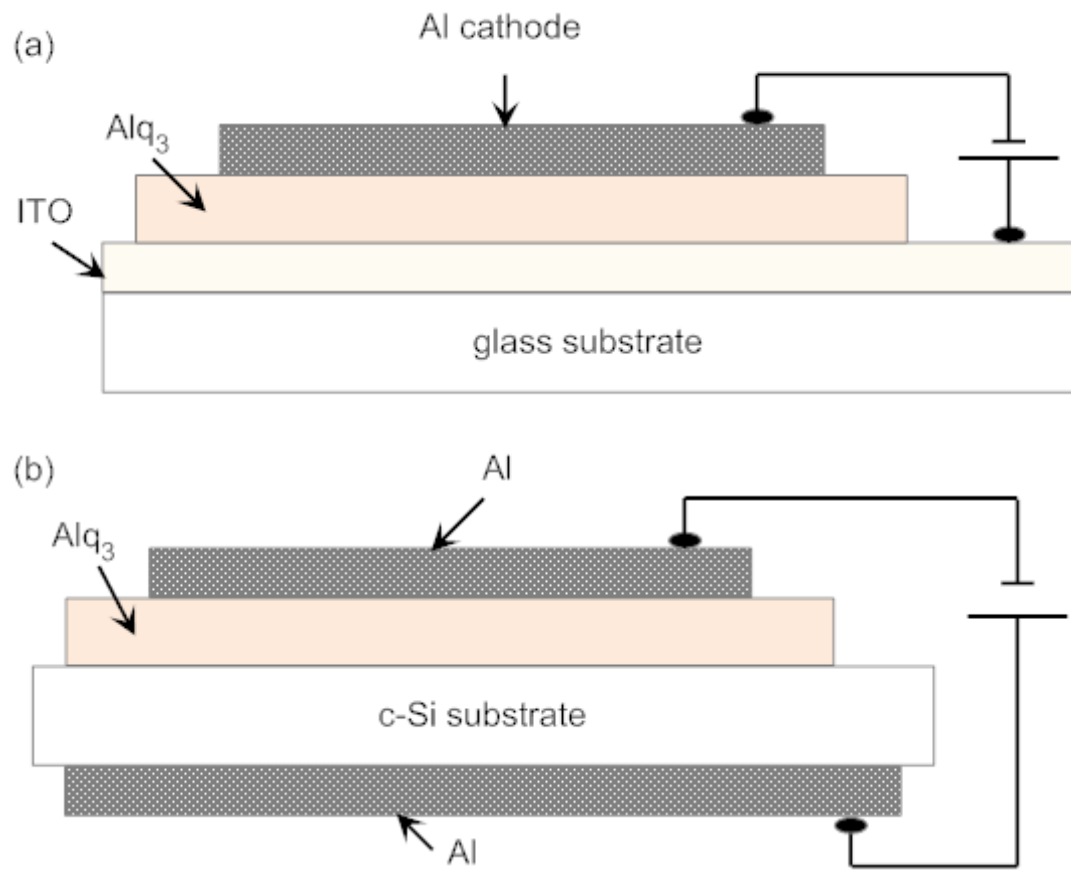
Fig. 3.3. (a) ITO/Alq$_3$/Al and (b) c-Si/Alq$_3$/Al devices structure configuration.

Chapter 4 Results and Discussions

4.1 Introduction

Experimental results and discussions on the photoluminescence and electrical properties of Alq_3 films deposited on ITO and c-Si substrates are presented in this chapter. It begins with displaying the photoluminescence properties Section 4.2 while the results for the electrical properties are presented in Section 4.3. These two section covered the effects of surface treatment on the anode material using various gases of methane (CH_4), helium (He), argon (Ar), oxygen (O_2) plasma, and UV/ozone (UV/O_3) treatment on the photoluminescence (PL) and electrical properties. Final part in Section 4.4, presents the discussions on the results.

4.2 Photoluminescence Properties

4.2.1 PL Emission Spectra of Alq_3 Films Deposited on ITO Substrates

Fig. 4.1 shows the PL emission spectra for Alq_3 films deposited on ITO substrates untreated and treated with CH_4, He, Ar, O_2 plasma, and UV/O_3 treatment for 1, 5, 10, and 20 minutes. It is obvious that the treatment time has significant effects on the PL emission spectra in terms of intensity and peak wavelength. UV/O_3 treatment on ITO substrates produced the highest PL emission intensity when the treatment time is 20 minutes while CH_4 plasma treatment on the ITO substrates irrespective of treatment time showed the most significant blue shift in the PL emission peak wavelength.
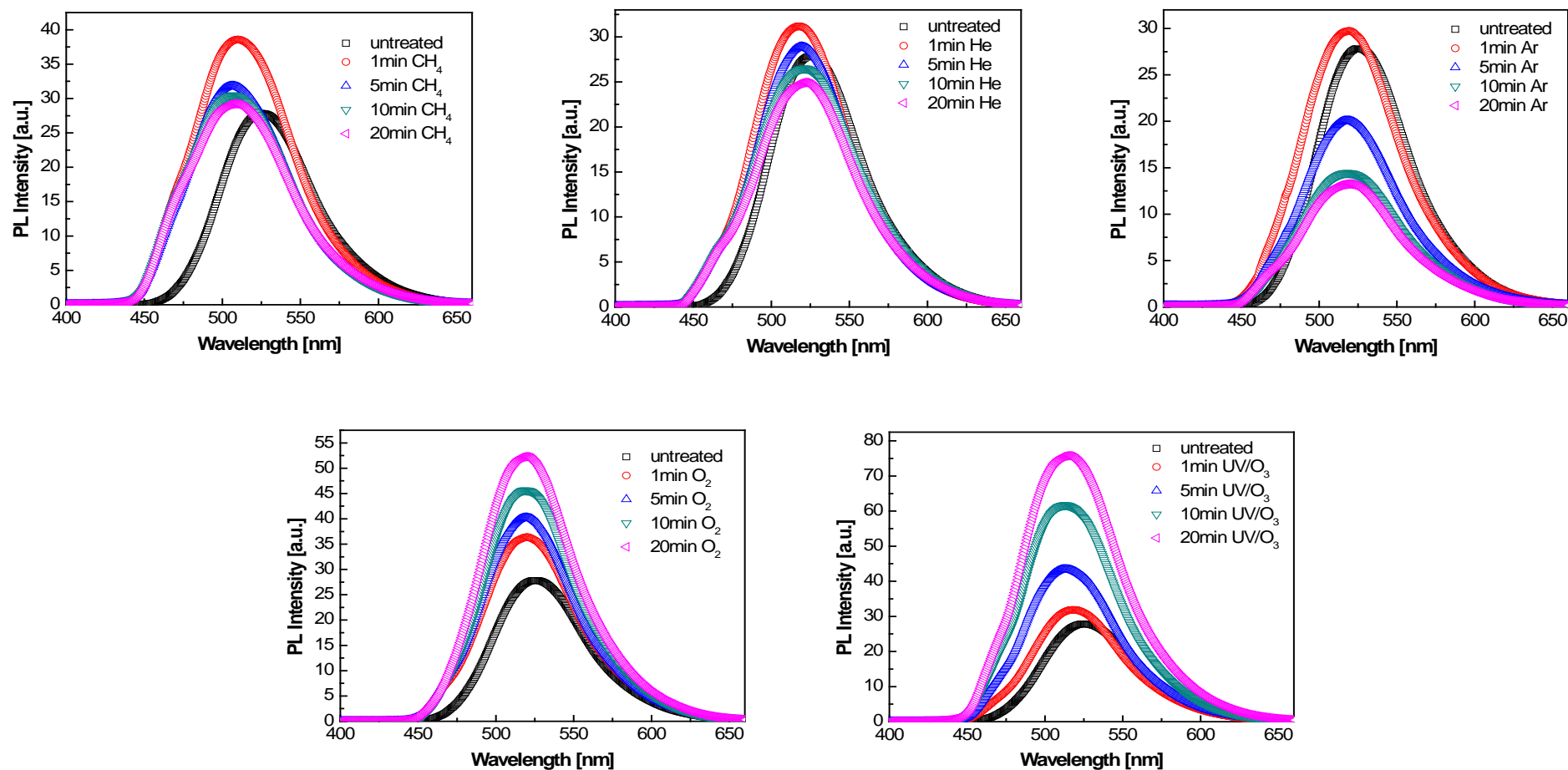
Fig. 4.1. PL emission spectra for Alq$_3$ films deposited on ITO substrates untreated and treated with CH$_4$, He, Ar, O$_2$ plasma, and UV/O$_3$ treatment for 1, 5, 10, and 20 min, respectively.

4.2.2 PL Emission Peak Intensity of Alq₃ Films on ITO Substrates: Effects of Surface Treatment Time on ITO Substrates Prior to Alq₃ Deposition
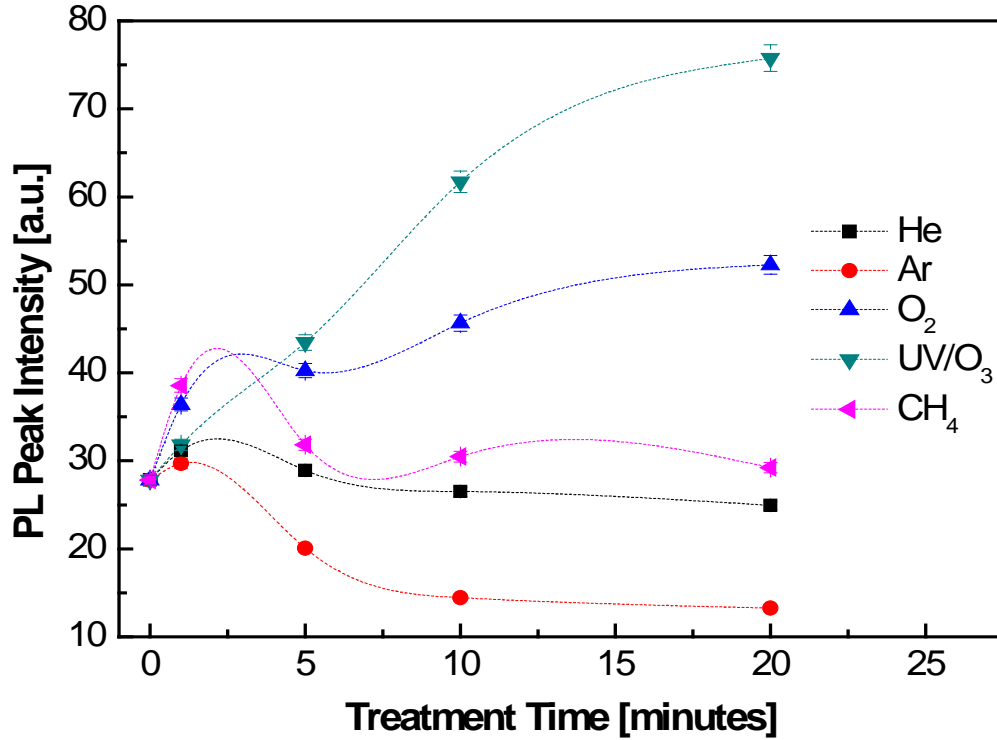
Fig 4.2. Effects of various ITO surface treatment time on the PL emission peak intensity of Alq₃ deposited on ITO substrate.

Fig. 4.2 shows the variation of PL emission peak intensity of Alq₃ films deposited on ITO substrates untreated and treated with CH₄, He, Ar, O₂ plasma, and UV/O₃ treatment for different time durations of 1, 5, 10, and 20 minutes. UV/O₃ treatment produced the most significant increase in PL emission intensity with increase in treatment time followed by O₂ plasma treatment. The PL emission intensity of the Alq₃ film on UV/O₃ treated ITO substrates increased at a faster rate when the treatment time is less than 10 minutes, but increased at a slower rate towards saturation when the treatment time is more than 10 minutes. UV/O₃ treatment on ITO substrates of Alq₃ films is very important in enhancing the PL emission intensity of Alq₃ films and longer

treatment time produces further enhancement in the PL emission intensity. In the case of O_2 plasma treatment, the highest PL emission intensity was obtained with 20 minutes of O_2 plasma treatment on the ITO substrates. CH_4 plasma treatment produced an increase in PL emission intensity when treated for a short duration of 1 minute. However, increase in CH_4 plasma treatment time on the ITO substrates to 20 minutes reduced the PL emission intensity to a constant low intensity. He and Ar plasma treatment on the ITO substrates produced a slight increase in PL emission intensity of the Alq_3 films when treated for 1 minute but the intensity dropped when the treatment time was increased beyond 1 minute. The decrease in the PL emission intensity was most obvious for the film deposited on ITO substrates treated with Ar plasma treatment.

UV/O_3 and O_2 plasma treatment involves incorporation of O atoms into the ITO structure at the surface thus increasing the presence of O atoms at the ITO/Alq_3 interface. The results above strongly indicate that higher O atom concentration at the interface has the effect of enhancing PL emission intensity of Alq_3 films. Long duration of CH_4 plasma treatment at the ITO surface increases the presence of hydrocarbon radicals (CH_2, CH_3, and CH) and secondary reactions further increases the presence of CH_3 radicals, the main deposition precursor of hydrogenated carbon (C:H) film. Thus, a thin layer of C:H film is expected to be present at the ITO/Alq_3 interface. Constant bombardment effects at the ITO surface by hydrocarbon ions also has significant effect on the roughness of the ITO surface. These effects degrade the PL emission intensity of the Alq_3 films. He and Ar plasma treatment constantly produce He^+ and Ar^+ ion bombardments on the ITO surface and is expected to introduce defective structures on the ITO surface. Ar^+ ion bombardments are more damaging to the ITO surface due to

the higher mass and the above results show that this degrades the PL emission intensity of Alq$_3$ films deposited on it. Defective structures at the ITO/Alq$_3$ interface as a result of ion bombardments on the ITO surface degrade PL emission intensity of Ar$^+$ ion films.

4.2.3 PL Emission Peak Position of Alq$_3$ Film on ITO Substrates: Effects of Surface Treatment Time on ITO Substrates Prior to Alq$_3$ Deposition

Fig 4.3. Effects of various ITO surface treatment time on the PL emission peak position of Alq$_3$ deposited on ITO substrate.
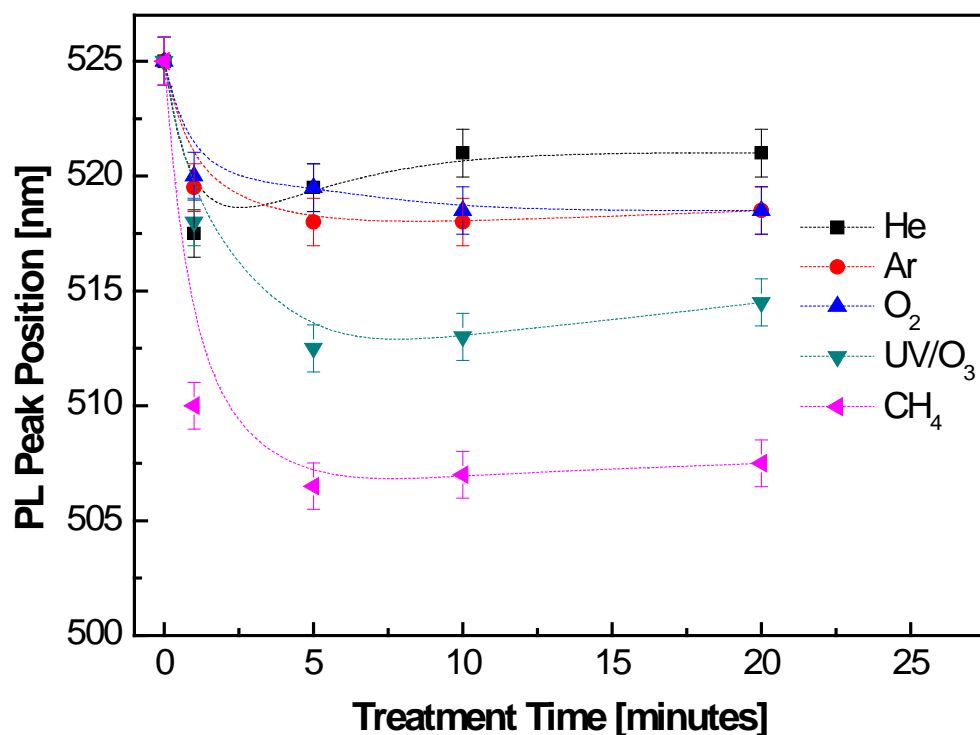
Fig. 4.3 show the effects of various ITO surface treatment time on the PL emission peak position of Alq$_3$ deposited on ITO substrates. Surface treatment of the ITO surface produced a blue shift in PL emission peak position of the Alq$_3$ films deposited on these ITO substrates. Increase in treatment time beyond 5 minutes produced no significant change in the PL emission peak positions of all films deposited on ITO substrates

except for the films deposited on ITO substrates treated with He plasma. In this case, the PL emission peak position decreases to a minimum when treated for 1 minute and further increase in treatment time produced a red shift in the PL emission peak position. The most significant blue shift is observed in the PL emission peak position of Alq_3 films deposited on ITO substrates treated with CH_4 plasma followed by the films deposited on ITO substrates treated with UV/O_3.

CH_4 plasma treatment forms a thin layer of C:H film at the ITO/Alq_3 interface and UV/ozone treatment incorporates high concentration of atoms at the interface forming a thin layer of indium oxide film at the interface. The formation of a layer of film at the interface which has a different structure from the ITO substrate and the Alq_3 film produces a significant blue shift in the PL emission peak position. The shift is more significant for Alq_3 film on CH_4 treated ITO as C:H film has a significantly different structure compared to ITO and Alq_3. Ar^+ and O^+ ion bombardments sputter atoms on the ITO surface etching away weak bonds. Since all the treatments are not done *in-situ*, exposure of the Ar treated ITO particularly attract O atoms from the atmosphere since it has higher dangling bonds concentration at the surface. O atoms are incorporated on the ITO surface during O_2 plasma treatment. However, the presence of O atoms on these ITO surface is not significant enough to change the ITO structure at the surface to form indium oxide film. Therefore, the shift in the PL emission peak positions is not as significant as the film on UV/O_3 treated ITO. He^+ ions are small in mass and therefore He^+ ion bombardments do not etch the surface atoms on the ITO. He plasma treatment longer than 1 minute create defects in the form of distortions of bonding structures at the surface thus creating states in the band gap of the ITO. This produces the red-shift in

the PL emission peak position of the Alq_3 film. The changes in the PL emission peak intensity and position show that PL emission from ITO/Alq_3 structures is strongly influenced by the properties of the ITO/Alq_3 interface.

4.2.4 PL Emission Spectra of Alq_3 Films Deposited on p-type c-Si Substrates

The PL emission spectra for Alq_3 films deposited on c-Si substrates untreated and treated with CH_4, He, Ar, O_2 plasma, and UV/O_3 treatment for 1, 5, 10, and 20 minutes are shown in Fig. 4.4. As in the films on ITO treated substrate, the surface treatment and the duration of treatment have influence on the PL emission intensity and peak position. The PL emission intensity of the Alq_3 films deposited on c-Si substrates are significantly lower than the intensity of the Alq_3 films deposited on ITO substrates. The highest PL emission intensity was obtained by the film on the UV/O_3 treated c-Si substrates with treatment time of 20 minutes while Ar plasma treatment on the c-Si substrates produced the most significant red shift phenomenon in PL emission peak position when treatment time was 20 minutes.
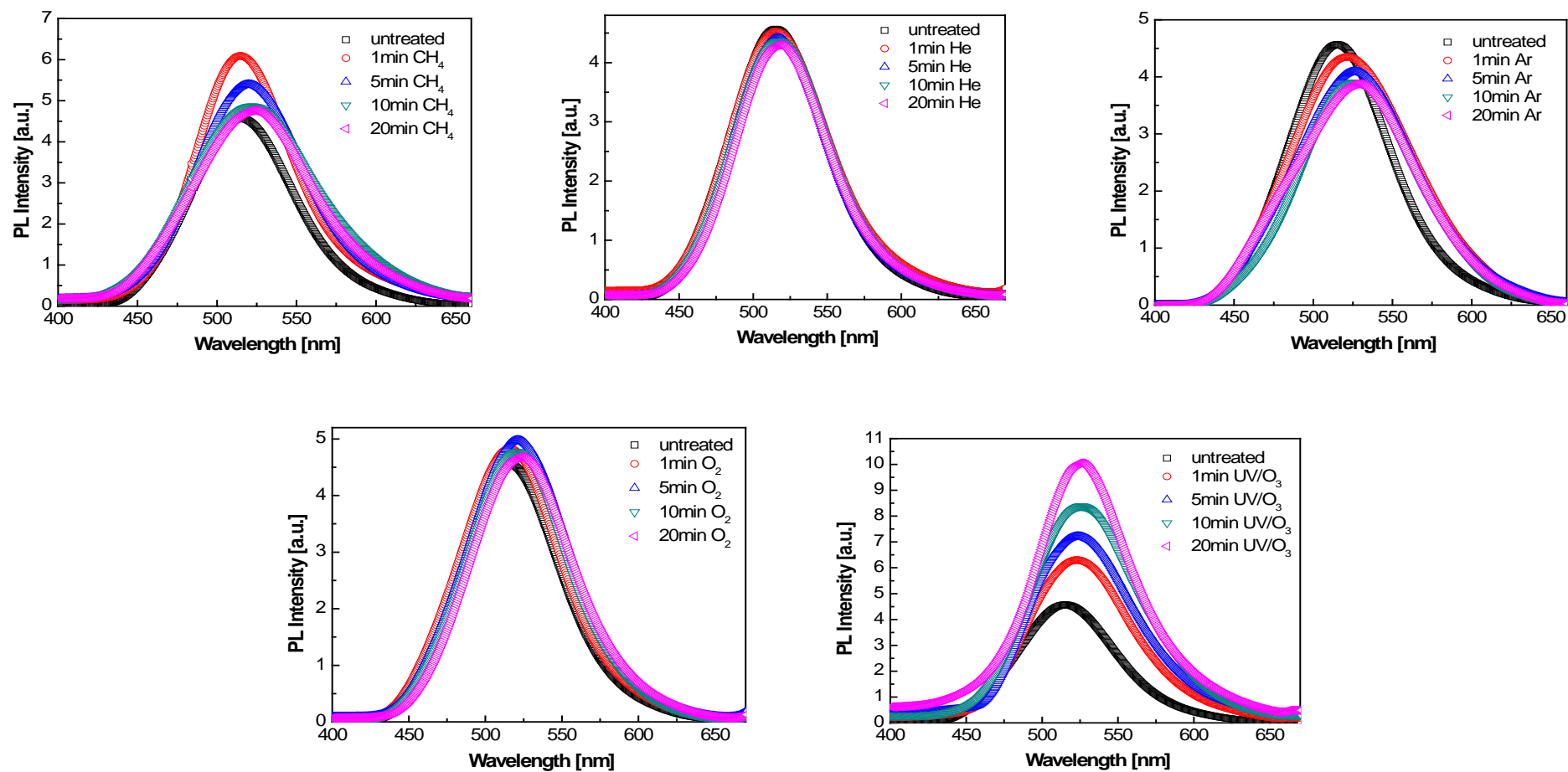
Fig. 4.4. PL emission spectra for Alq$_3$ films deposited on c-Si substrates untreated and treated with CH$_4$, He, Ar, O$_2$ plasma, and UV/O$_3$ treatment for 1, 5, 10, and 20 min, respectively.

4.2.5 PL Emission Peak Intensity of Alq₃ Films on p-type c-Si Substrates: Effects of Surface Treatment Time on p-type c-Si Substrates Prior to Alq₃ Deposition

The variation of PL emission peak intensity of Alq$_3$ films deposited on c-Si substrates untreated and treated with CH$_4$, He, Ar, O$_2$ plasma, and UV/O$_3$ treatment for different time durations of 1, 5, 10, and 20 minutes is shown in Fig. 4.5. The Alq$_3$ film on the c-Si substrates treated with UV/O$_3$ treatment produced the most significant increase in PL emission intensity with increase in treatment time. Thus, UV/O$_3$ treatment on c-Si substrates of Alq$_3$ films enhanced the PL emission intensity of Alq$_3$ film. For CH$_4$ plasma treatment, the PL emission intensity significantly was increased when c-Si substrates were treated for 1 minute.
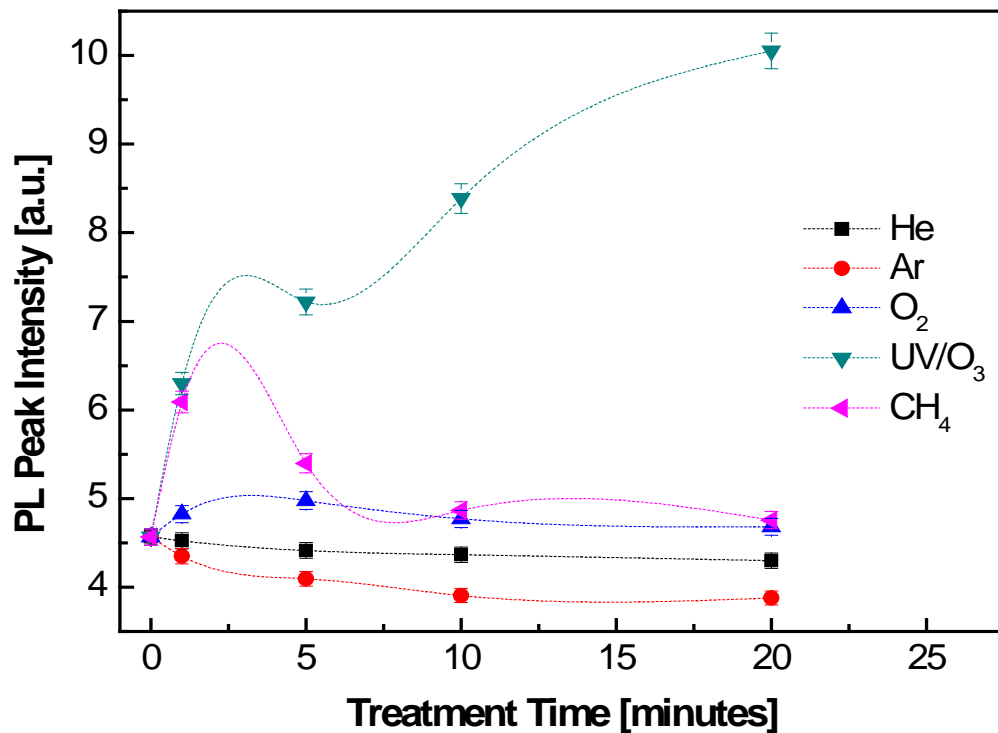
Fig 4.5. Effects of various c-Si surface treatment time on the PL emission peak intensity of Alq$_3$ deposited on c-Si substrate.

However, further increase in treatment time beyond 1 minute decreased the PL emission intensity to a low value. PL emission intensity shows very little change when the c-Si surface was treated with He and O_2 plasma treatments. Ar plasma treatment on c-Si substrates degraded the PL emission intensity for the film.

As in the case of UV/O_3 surface treatments on the ITO substrates, UV/O_3 treatment on c-Si substrates also significantly enhanced the PL emission intensity of Alq_3 film while Ar plasma treatment on the c-Si substrates degraded the PL emission intensity. For the film on the O_2 treated ITO substrates, the PL emission intensity increased noticeably with treatment time, however, for the film on the O_2 treated c-Si substrates, produced no significant change in PL emission intensity. He plasma treatment did not produce much change in the PL emission intensity for both Alq_3 film on ITO and c-Si substrates. From the results, PL emission intensity of Alq_3 film on c-Si substrates is enhanced when high concentration of O atoms is incorporated into the c-Si surface by the UV/O_3 treatment. Ar plasma treatment degrades PL emission intensity of Alq_3 film on c-Si substrates as a result of the dominant presence of structural defects on the c-Si surface.

4.2.6 PL Emission Peak Position of Alq$_3$ Films on p-type c-Si Substrates: Effects of Surface Treatment Time on p-type c-Si Substrates Prior to Alq$_3$ Deposition
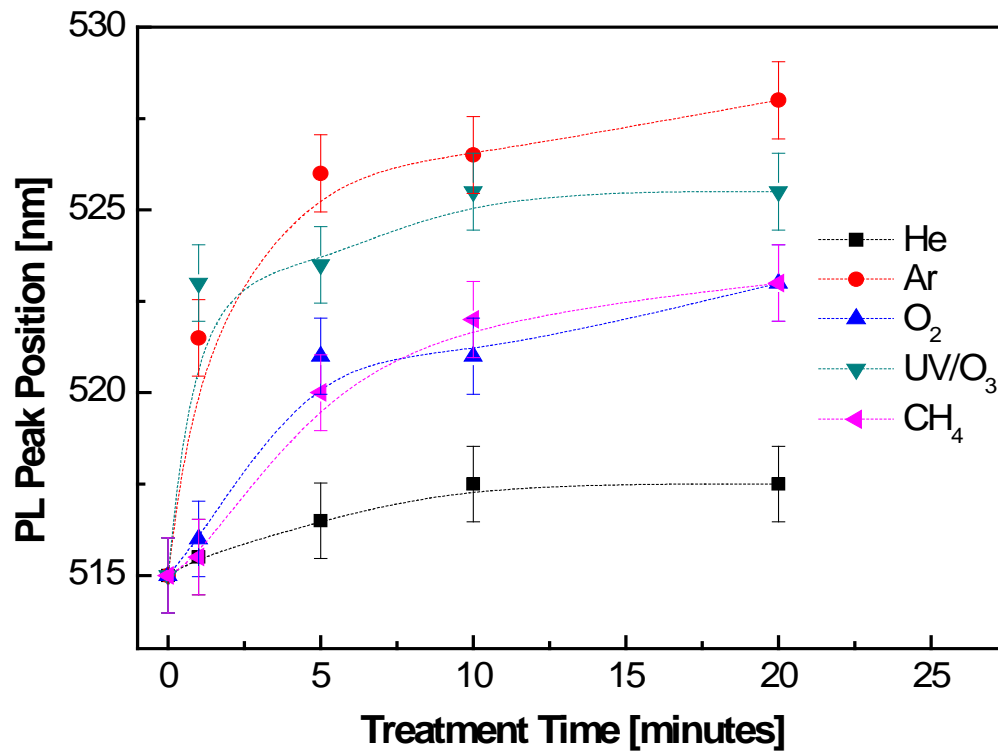
Fig 4.6. Effects of various c-Si surface treatment time on the PL emission peak position of Alq$_3$ deposited on c-Si substrate.

Fig. 4.6 shows the effects of various c-Si surface treatment time on the PL emission peak position of Alq$_3$ deposited on c-Si substrates. The Alq$_3$ film on ITO substrates generally produced a blue shift in the PL emission peak position when the ITO surface was treated with CH$_4$, Ar, O$_2$ plasma, and UV/O$_3$. However, for Alq$_3$ film on c-Si substrates generally a red shift phenomenon in the PL emission peak position of the Alq$_3$ film was observed when the surface of the c-Si substrates were treated using the above treatments. The most significant red-shifted in PL emission peak position was obtained by the Alq$_3$ film on the c-Si substrates treated with Ar plasma treatment

followed by UV/O_3 treatment. The shift for the He plasma treated c-Si substrates was least significant as compared to the other surface treatments. However, it is noted that treatment times beyond 5 minutes produced no further shift in PL emission peak positions of all Alq_3 film on c-Si substrates.

Obviously, the PL emission in Alq_3 films on c-Si substrates is mainly contributed by recombination of electron-hole pairs in defect states at c-Si/Alq_3 interface. Ar plasma treatment produced the highest defect density as a result of intense Ar^+ ion bombardment on the c-Si surface, thus the most significant red shift in the PL peak position.

UV/O_3 treatment and O_2 plasma treatment produced defect density in the form of impurities O atoms on the c-Si surface and as shown by the results above, also produced the next most significant red shift in the PL emission peak position. Similarly, CH_4 plasma treatment introduced defects in the form of C atoms that produced the red shift in the PL emission peak position. He atom being the smallest atom as compared to the other atoms involved in the other treatments, comparatively less defects to the c-Si surface, thus showed very little change in the PL emission peak position.

4.3 Electrical Properties

4.3.1 Current-Voltage Plots of ITO/Alq_3/Al Heterostructure

Fig 4.7 shows the current-voltage (I-V) characteristics for ITO/Alq_3/Al heterostructure with the ITO anode untreated and treated with CH_4, He, Ar, O_2 plasma, and UV/O_3 treatment for 1, 5, 10, and 20 minutes, prior to the Alq_3 film deposition. The threshold voltages (V_T) of the ITO/Alq_3/Al heterostructures generally were significantly

lowered when the ITO anodes were treated with He, Ar, O_2 plasma, and UV/O_3 compared to the heterostructure with untreated ITO. The $ITO/Alq_3/Al$ heterostructure with the lowest V_T was the UV/O_3 treated ITO heterostructure followed by the O_2, He, and Ar plasma treated ITO heterostructure. However, the heterostructure with the He and Ar plasma treated ITO showed an increase in V_T when the ITO treatment time was longer than 5 minutes. The heterostructure with CH_4 plasma treated ITO however produced an increase in V_T with increase in treatment time.
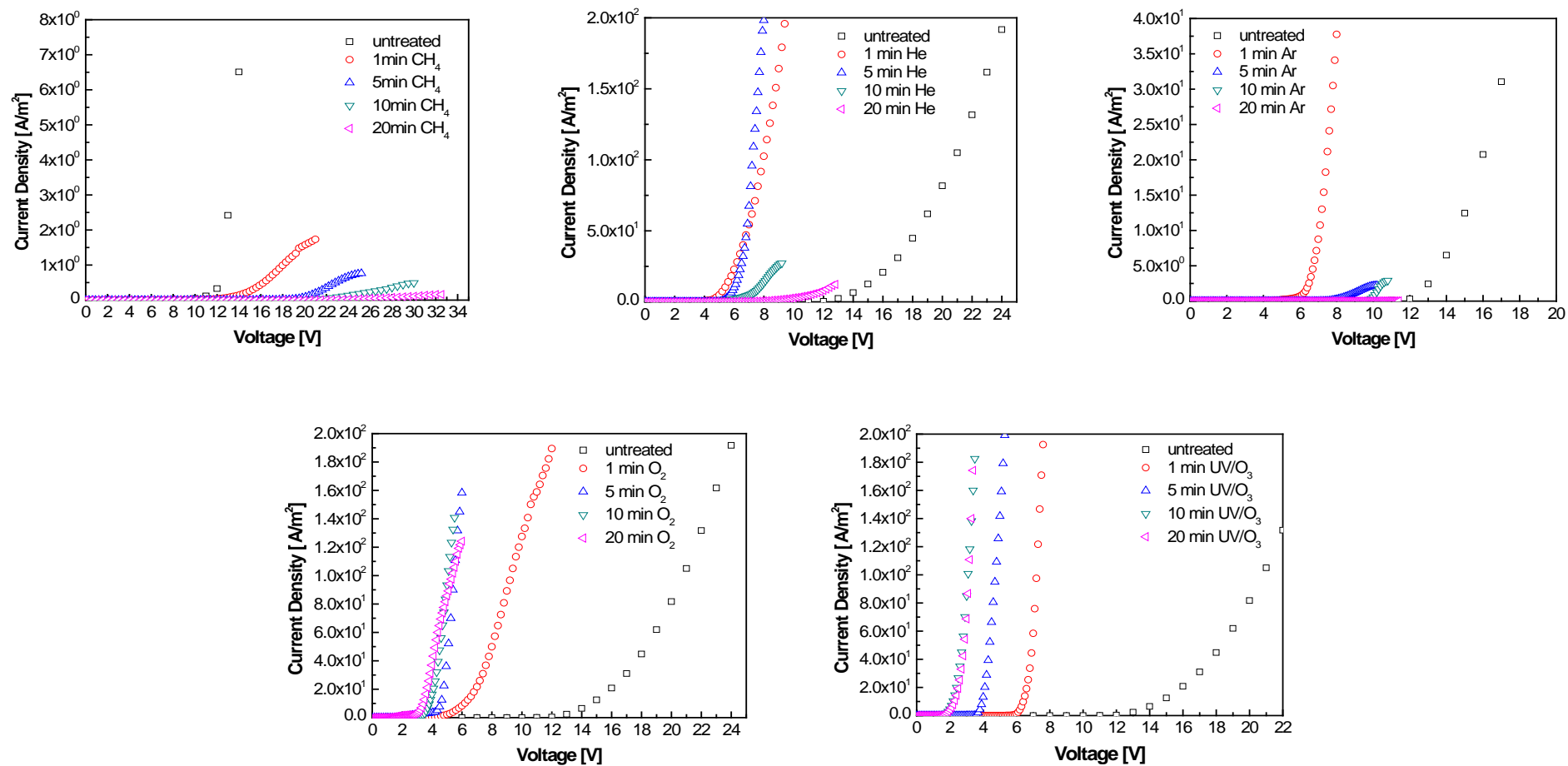
Fig. 4.7. Current-voltage characteristics for Alq$_3$ films deposited on ITO substrates untreated and treated with CH$_4$, He, Ar, O$_2$ plasma, and UV/O$_3$ treatment for 1, 5, 10, and 20 min, respectively.

4.3.2 Threshold Voltage: ITO/Alq$_3$/Al Heterostructure
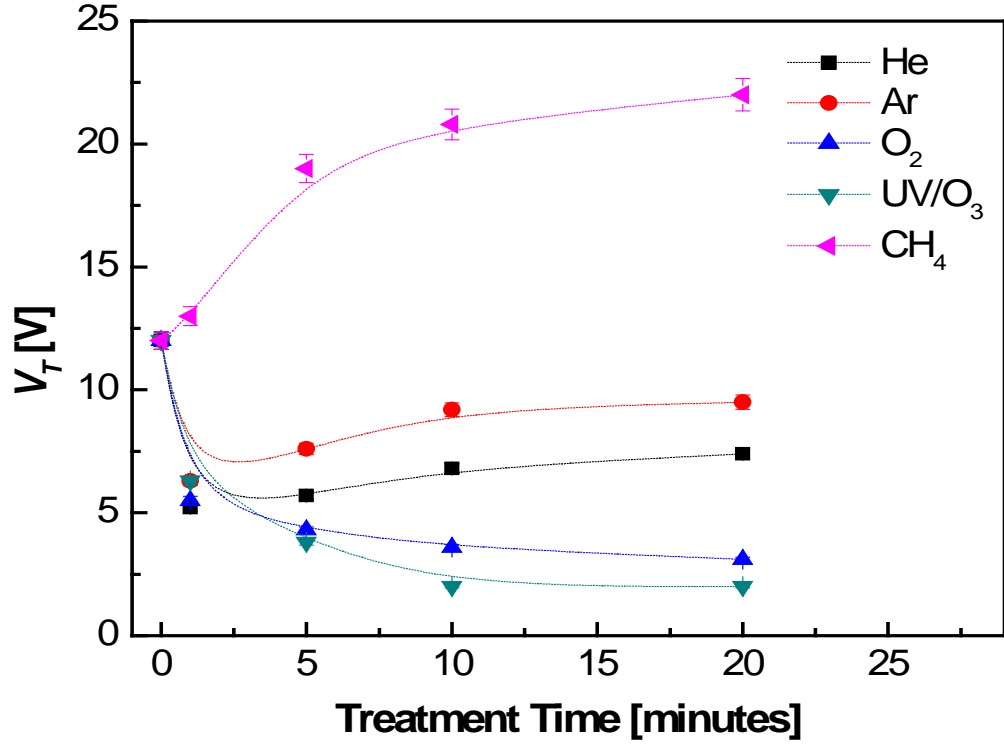
Fig 4.8. Variation of threshold voltage (V_T) with treatment time for ITO/Alq$_3$/Al heterostructure.

Fig 4.8 shows the variation of V_T with treatment time for ITO/Alq$_3$/Al heterostructure with the ITO anode untreated and treated with CH$_4$, He, Ar, O$_2$ plasma, and UV/O$_3$ treatment for 1, 5, 10, and 20 minutes, prior to the Alq$_3$ film deposition. As mentioned in Section 4.6.1, short duration He, Ar, O$_2$, and UV/O$_3$ treatments of 1 minute done on the ITO surface have the significant effect of lowering V_T for all the ITO/Alq$_3$/Al heterostructures. V_T for the heterostructure with He and Ar plasma treated ITO decreased to 5.2 and 6.3 V, respectively when the treatment time duration was 1 minute. The He and Ar plasma treated ITO showed an increase in V_T for the heterostructure to 7.4 and 9.5 V, respectively when the treatment time was increased to 5 minutes or longer. CH$_4$ plasma treatment on the ITO surface on the other hand increased

V_T with increase in CH_4 plasma treatment time. V_T increased from 12 to 22.6 V with the increase in ITO treatment time to 20 minutes. UV/O_3 treated ITO heterostructure produced the most significant decrease in V_T to 2 V followed by O_2 plasma treated ITO heterostructure where V_T decreased to 3 V when the ITO treatment time was increased to 20 minutes.

UV/O_3 and O_2 plasma treatments on the ITO produced significant decrease in V_T for the heterostructure with increase in treatment time. This shows that O atoms incorporation into the ITO surface structure has the effect of increasing the V_T for the heterostructure. Short duration of He and Ar plasma treatments on the ITO also produced a decrease in V_T as a result of removal of hydrocarbon contamination on the ITO surface. Long duration of He and Ar plasma treatments on the ITO produced defecting structures on the ITO surface as a result of ion bombardments and this has the effect of increasing the V_T for the heterostructure. The formation of carbon film on the ITO surface due the discharge of CH_4 plasma significantly increased the V_T for the heterostructure.

4.3.3 Threshold Current: ITO/Alq$_3$/Al Heterostructure

The variation of threshold current (J_T) with treatment time for ITO/Alq$_3$/Al heterostructure after ITO substrates are subjected to CH_4, He, Ar, O_2 plasma, and UV/O_3 treatment of 0, 1, 5, 10, and 20 minutes, prior to the Alq$_3$ film deposition are shown in Fig. 4.9. The highest J_T of 7.31 A/m^2 was obtained for the heterostructure with the ITO treated with He plasma for 1 minute. The UV/O_3, O_2, and Ar plasma treatments on ITO also showed maximum J_T when the ITO for the heterostructure was treated for 1 minute

in the order of 5.86, 4.98 and 1.5 A/m^2, respectively. However, J_T significantly

decreased when the treatment time was extended beyond 5 minutes. The O$_2$ plasma and

UV/O$_3$ treatment on the ITO decreased the J_T to 4.21 and 4.45 A/m^2 respectively when

the ITO was treated for 20 minutes. The decrease in J_T for the He and Ar plasma treated

ITO heterostructure produced a significant decrease in J_T to 0.43 and 0.002 A/m^2

respectively when the ITO was treated for 20 minutes. The lowest J_T of 0.005 A/m^2 was

obtained by the CH$_4$ plasma treated ITO heterostructure with 20 minutes of treatment

time.
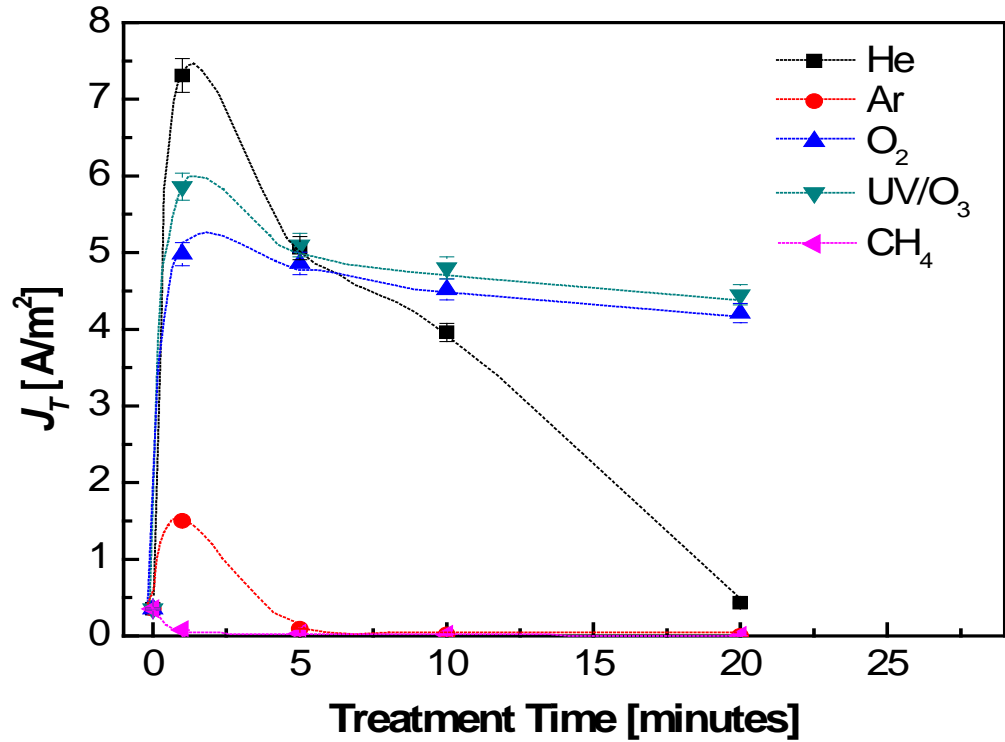
Fig 4.9. Variation of threshold current (J_T) with treatment time for ITO/Alq$_3$/Al
heterostructure.

Ion bombardment effect as a result from the He and Ar plasma treatments on the

ITO surface produced cleaning effect on the ITO surface when duration of these

treatments is short. However, J_T for He plasma treated ITO heterostructure is enhanced

significantly when treated for a short time duration compared to Ar plasma treated ITO heterostructure. This is due to the higher bombardment effect produced by Ar^+ ions which may creates both cleaning as well as destructive structural effects on the ITO surface. Incorporation for the UV/O_3 and O_2 plasma treatments clearly produced high J_T even when the ITO was treated for long time duration. Incorporation of carbon contamination layer on the ITO surface has the adverse effect of decreasing J_T to a very low value.

4.3.4 OLED Driving Voltage: ITO/Alq$_3$/Al Heterostructure

The V_d is the voltage required to produce OLED current density of 3 A/m^2. The objective of this analysis is to obtain the best ITO surface treatment for ITO/Alq$_3$/Al heterostructure for OLED applications. Fig. 4.10 show the variation of V_d with treatment time for ITO/Alq$_3$/Al heterostructure after the ITO surface treatments using CH_4, He, Ar, O_2 plasma, and UV/O_3 treatment, prior to the Alq$_3$ deposition. V_d for CH_4 and Ar plasma treated ITO heterostructure was very large such that it can only be recorded when the ITO treatment time for the heterostructure up to 10 minutes. He plasma treated ITO heterostructure decreased the V_d to 4.8 V when the treatment time duration was 1 minute and increased to 10.1 V when the treatment time was increase to 20 minutes. The lowest V_d was obtained using UV/O_3 treatment followed by the O_2 plasma treatment on the ITO heterostructure with increase in treatment time. V_d for the heterostructure with UV/O_3 and O_2 plasma treatment on the ITO decreased from 13.1 to 1.91 and 2.95 V, respectively when the treatment time duration was 20 minutes.
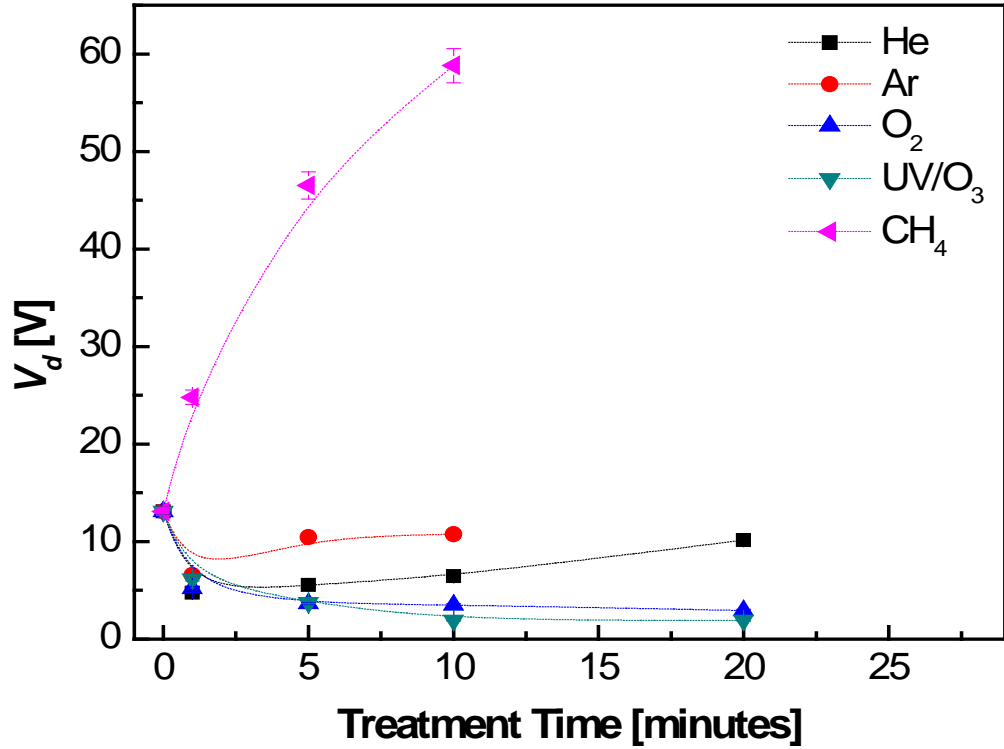
Fig 4.10. Variation of OLED driving voltage (V_d) with treatment time for ITO/Alq$_3$/Al heterostructure.

V_d for UV/O$_3$ and O$_2$ plasma treated ITO heterostructure is reduced significantly with increase in treatment time. This indicates that the incorporation of O atoms in the ITO surface structure has the effect of reducing the V_d for the heterostructure. V_d for the heterostructure of He and Ar plasma treated ITO for short duration was decreased as a result of removal of hydrocarbon contamination on the ITO surface. He and Ar plasma treatment produce the ion bombardments on the treated ITO creating defecting structures on the ITO surface and this increasing the V_d for the heterostructure. CH$_4$ plasma treatment on the ITO produced the increase in V_d for the heterostructure as a result of formation of carbon film on the ITO surface.

4.3.5 Fowler-Nordheim Plots of ITO/Alq$_3$/Al Heterostructure

Fig. 4.11 shows the Fowler-Nordheim (FN) plots of ITO/Alq$_3$/Al heterostructure derived from the *I-V* plots in Fig. 4.7. The derivation of FN plots from *I-V* plots was detailed in Section 2.5. The FN plots is used to determine the hole injection barrier (Φ_h) at the ITO/Alq$_3$ interface by using Eq. (2.9). The linear part of the FN plot shifted to higher field with increase in CH$_4$ plasma treatment time to 20 minutes while the linear part of the FN plots shifted to lower field after He, Ar, O$_2$ plasma, and UV/O$_3$ treatment. UV/O$_3$ treatment on the ITO surface shifted the linear part in the FN plots to the lowest field value followed by O$_2$ plasma treatment when the treatment time is 20 minutes. He and Ar plasma treatments on the ITO surface only shifted the linear part of the FN plots to a high inverse field value only when the ITO surface is treated for short time duration of 1 minute.
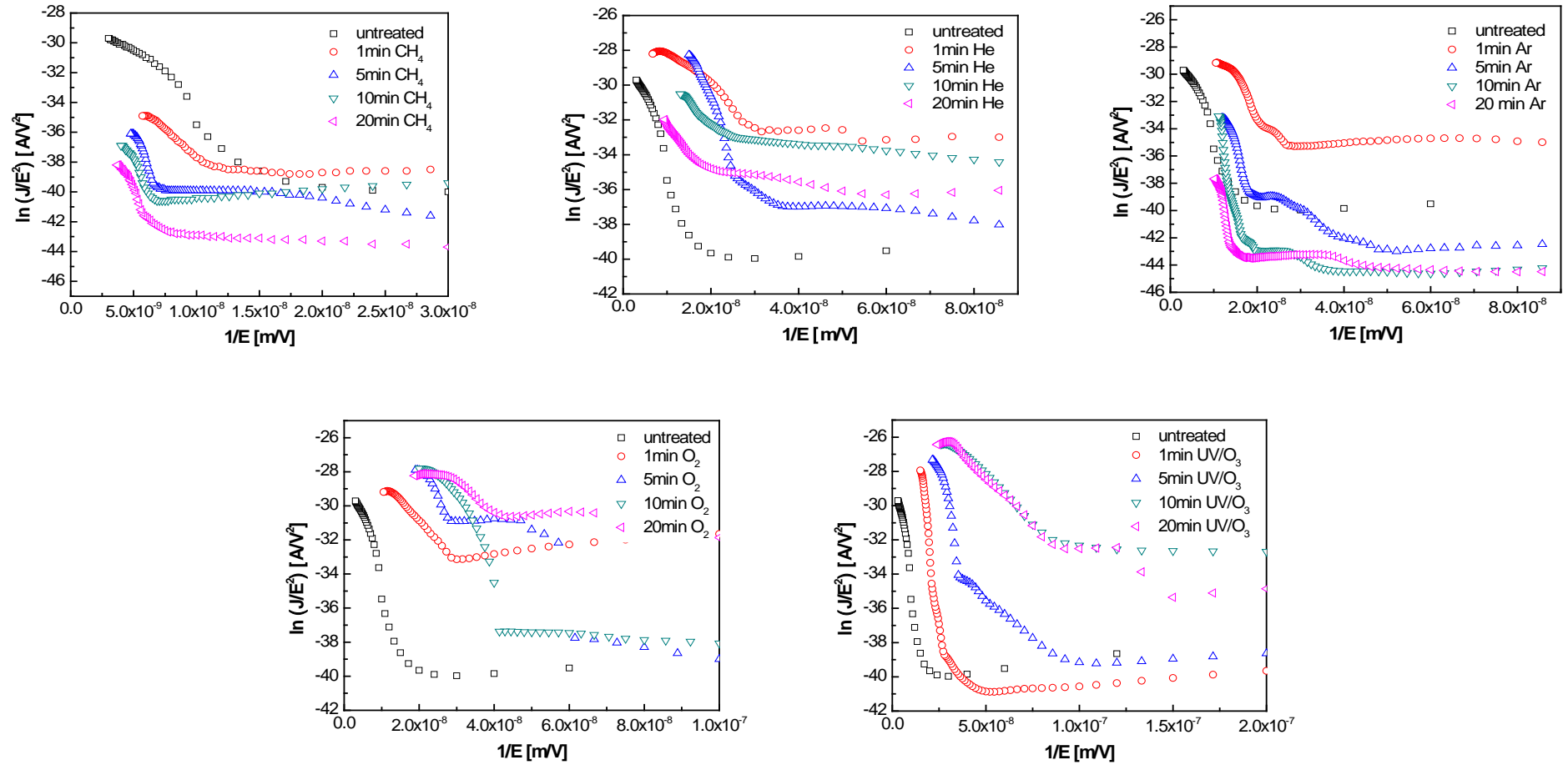
Fig. 4.11. Fowler-Nordheim plots for ITO/Alq$_3$/Al heterostructure where the Alq$_3$ films were deposited on the untreated ITO substrates and ITO substrates treated with CH$_4$, He, Ar, O$_2$ plasma, and UV/O$_3$ treatment for 1, 5, 10, and 20 min, respectively.

4.3.6 Hole Injection Barrier: ITO/Alq$_3$/Al Heterostructure

Fig. 4.12 shows the variation of barrier height (Φ_B) with treatment time for ITO/Alq$_3$/Al heterostructure with ITO substrates untreated and treated with CH$_4$, He, Ar, O$_2$ plasma, and UV/O$_3$ treatment of 0, 1, 5, 10, and 20 minutes, prior to the Alq$_3$ film deposition. Since these treatments were done on the ITO substrates, Φ_B is the hole injection barrier (Φ_h) at the ITO/Alq$_3$ interface as the electron injection barrier (Φ_e) is expected to produce no change with these treatments done on the ITO substrates. The highest Φ_B for the heterostructure was obtained with CH$_4$ plasma treatment on the ITO surface. Φ_B for the heterostructure significantly increase to 0.48 eV with increase in treatment time to 5 minutes and further increase in treatment time to 20 minutes produced a slow increase in Φ_B for the heterostructure. UV/O$_3$ treated ITO surface produced the lowest Φ_B for the heterostructure. Φ_B for the heterostructure significantly decreased from 0.12 to 0.06 eV with increase in treatment time to 20 minutes. Similarly, Φ_B for the heterostructure with O$_2$ plasma treated ITO decreased to 0.09 eV with increase in treatment time to 20 minutes. In the case of He and Ar plasma treatment, both treatments behaved similarly, i.e. Φ_B for the heterostructure decreased to a minimum of 0.08 and 0.09 eV, respectively with treatment time of 1 minute and increased to higher value of 0.13 eV (He and Ar) with increase in treatment times to 20 minutes.
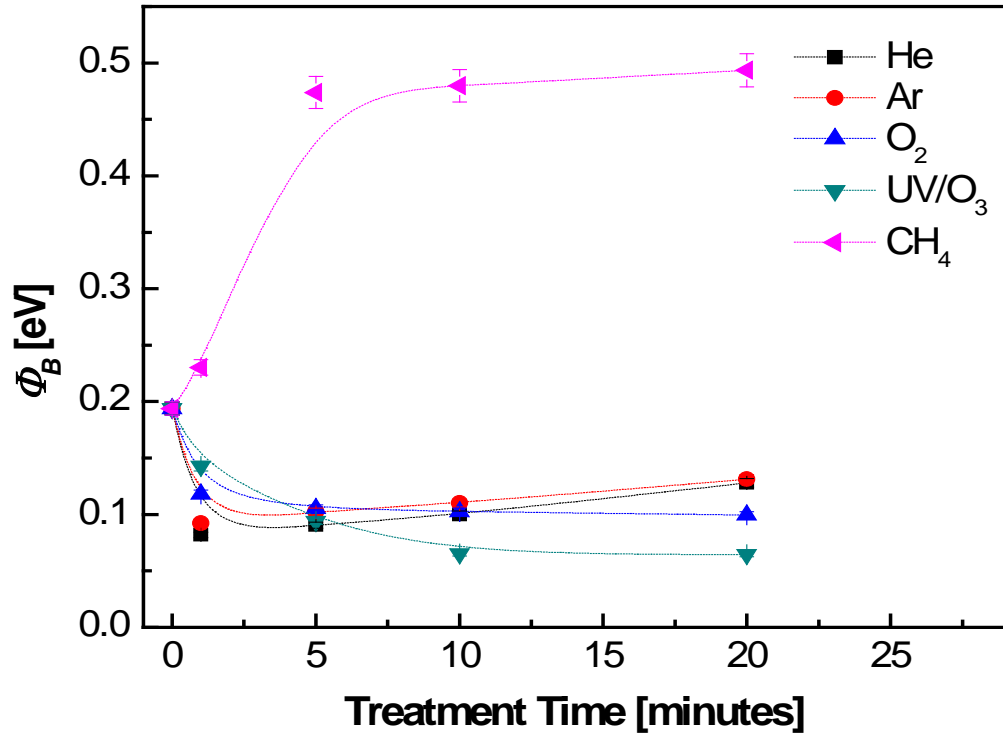
Fig 4.12. Variation of barrier height (Φ_B) with treatment time for ITO/Alq$_3$/Al heterostructure.

Φ_B for the heterostructure significantly increased with CH$_4$ plasma treated the ITO surface as a result of the formation of carbon layer on the ITO surface. Incorporation of O atoms into the ITO surface of the UV/O$_3$ and O$_2$ plasma treatment on the ITO heterostructure has the effect of decreasing the Φ_B for the heterostructure. Short duration of He and Ar plasma treatments on the ITO heterostructure produced a cleaning effects on the ITO surface reducing the Φ_B for the heterostructure. Long duration of He and Ar plasma treatments on the ITO heterostructure produced ion bombardment effects on the ITO surface and created structural defects on the ITO surface increasing the Φ_B for the heterostructure.

4.3.7 Current-Voltage Plots of c-Si/Alq$_3$/Al Heterostructure

The *I-V* characteristics for Alq$_3$ films deposited on c-Si substrates untreated and treated with CH$_4$, He, Ar, O$_2$ plasma, and UV/O$_3$ treatment for 1, 5, 10, and 20 minutes, prior to the Alq$_3$ film deposition are shown in Fig. 4.13. Treating the c-Si anodes with O$_2$ plasma and UV/O$_3$ treatment produced lower V_T of c-Si/Alq$_3$/Al heterostructure compared to the untreated c-Si heterostructrure. V_T for CH$_4$ plasma treatment on c-Si heterostructure significantly increased to higher value with increase in treatment time and also produced the highest value in V_T. V_T for the heterostructure decreased to a minimum with 1 minute He and Ar plasma treatment on the c-Si surface and increased to a higher value in V_T when the treatment times were increased beyond 5 minutes.
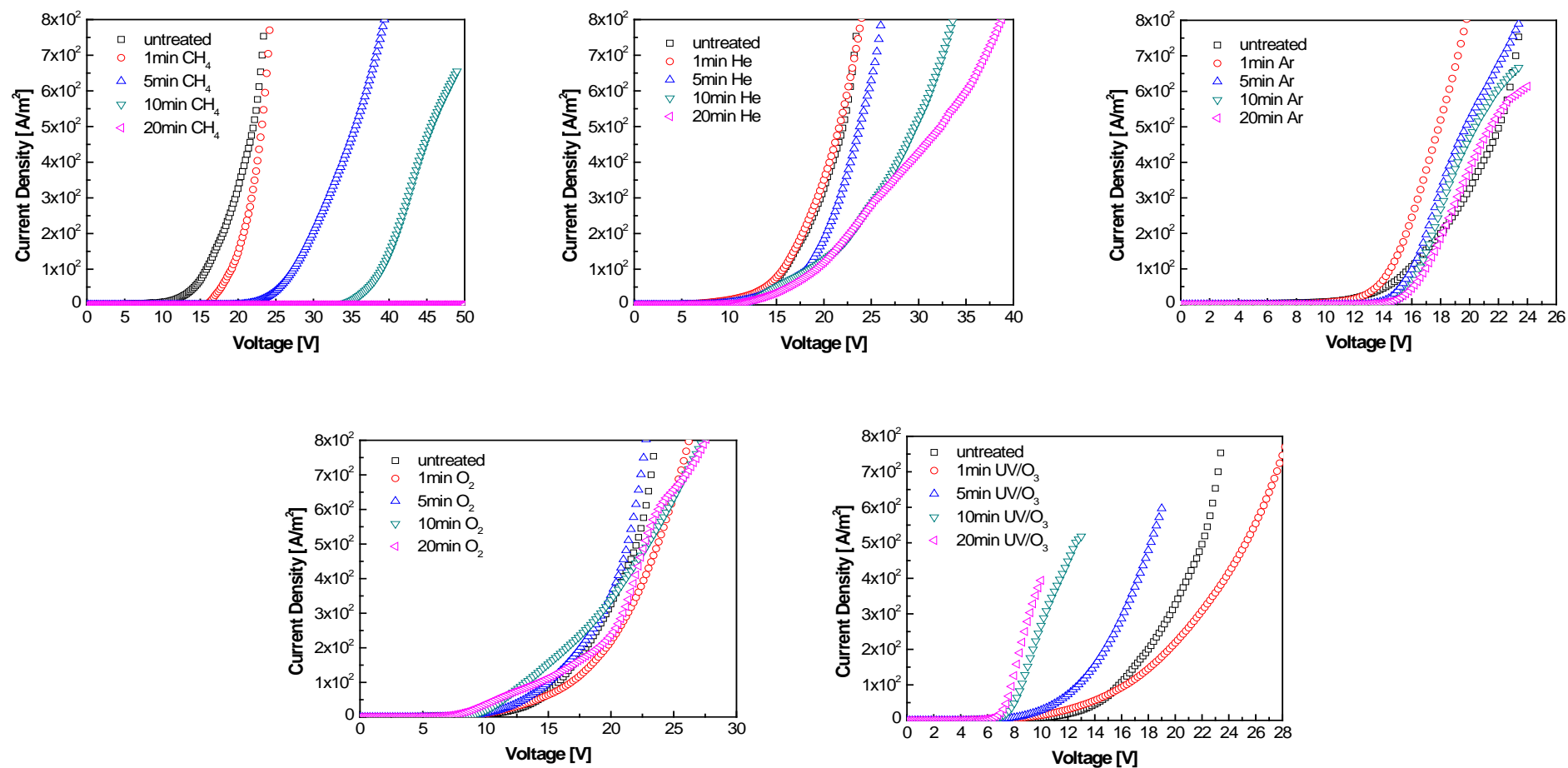
Fig. 4.13. Current-voltage characteristics for Alq$_3$ films deposited on c-Si substrates untreated and treated with CH$_4$, He, Ar, O$_2$ plasma, and UV/O$_3$ treatment for 1, 5, 10, and 20 min, respectively.

4.3.8 Threshold Voltage: c-Si/Alq₃/Al Heterostructure
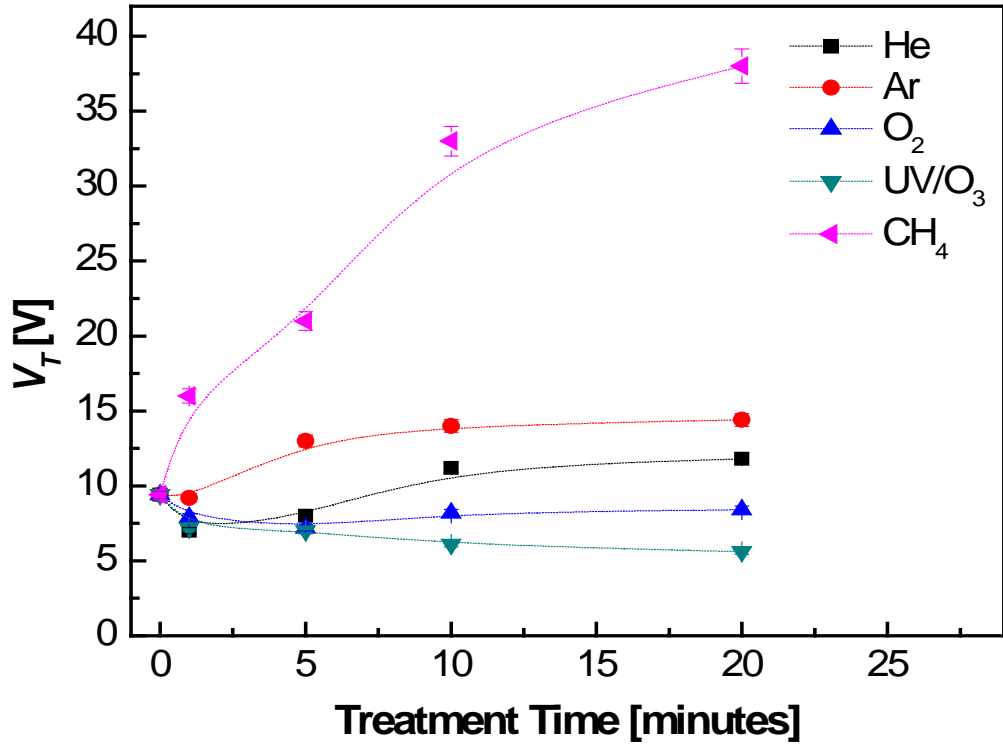
Fig 4.14. Variation of threshold voltage (V_T) with treatment time for c-Si/Alq$_3$/Al heterostructure.

Fig. 4.14 displays the variation of V_T with treatment time for c-Si/Alq$_3$/Al heterostructure with similar surface treatments on the ITO substrates as mentioned in Fig. 4.69. The V_T value for untreated c-Si heterostructure is 9.4 V. V_T for the heterostructure with CH$_4$ plasma treated c-Si significantly increased from 9.4 to 38 V with increase in treatment time to 20 minutes. V_T for the heterostructure with He and Ar plasma treatment on the c-Si decreased to 7 and 8.8 V, respectively when the treatment time duration was 1 minute. However, when the He and Ar plasma treatment time was prolonged beyond 5 minutes, V_T for the heterostructure increased to 11.8 and 14.4 V, respectively. V_T for O$_2$ plasma treated c-Si heterostructure decreased to 7.2 V when treatment time was 5 minutes and further increase the treatment time to 20 minutes,

increases the V_T to 8.4 V for the heterostructure. UV/O$_3$ treatment produced the most significantly decrease in V_T for the heterostructure with increase in UV/O$_3$ treatment time. The lowest V_T value of 5.6 V for the heterostructure was obtained with UV/O$_3$ treatment on the c-Si surface.

Incorporation of O atoms into the ITO surface of the UV/O$_3$ treatments clearly has the effect of decreasing the V_T for the heterstructure. Short duration of He and Ar plasma produced a cleaning effect by removal of hydrocarbon contaminants on the c-Si surface and decreased the V_T for the heterostructure. Long duration of He and Ar plasma produced the ion bombardment effects that created defecting structures on the c-Si and increased the V_T for the heterostructure. V_T for the heterostructure significantly increased due to the formation of carbon layer on the c-Si surface as a result of the discharge of CH$_4$ plasma. V_T for O$_2$ plasma treated c-Si heterostructure was decreased when treated for long time duration. This could be due to the more dominant O$^+$ ion bombardments effects on the c-Si surface during the long duration treatment compared to the incorporation of the O atoms into the c-Si surface.

4.3.9 Threshold Current: c-Si/Alq$_3$/Al Heterostructure

Fig. 4.15 shows the variation of J_T with treatment time for c-Si/Alq$_3$/Al heterostructure with similar surface treatments using CH$_4$, He, Ar, O$_2$ plasma, and UV/O$_3$ treatment on the ITO substrates as mentioned in Fig. 4.71. J_T for UV/O$_3$ treated c-Si heterostructure decreased to 2.8 A/m^2 with increase in treatment time to 20 minutes. Ar plasma treated c-Si heterostructure showed the minimum value of 2.3 A/m^2 when treatment duration was 1 minutes. He, and O$_2$ plasma treated c-Si heterostructure also

showed a minimum value of 1.8 and 1.3 A/m^2, respectively when treatment duration was 5 minute. However, increase in He, Ar, and O$_2$ treatment times to 20 minutes significantly increased the J_T value of 6.5, 6.7, and 7.3 A/m^2, respectively for the heterostructure. J_T of 1×10^{-5} A/m^2 for the heterostructure of CH$_4$ plasma treated c-Si heterostructure was the lowest with increase the treatment time to 20 minutes.
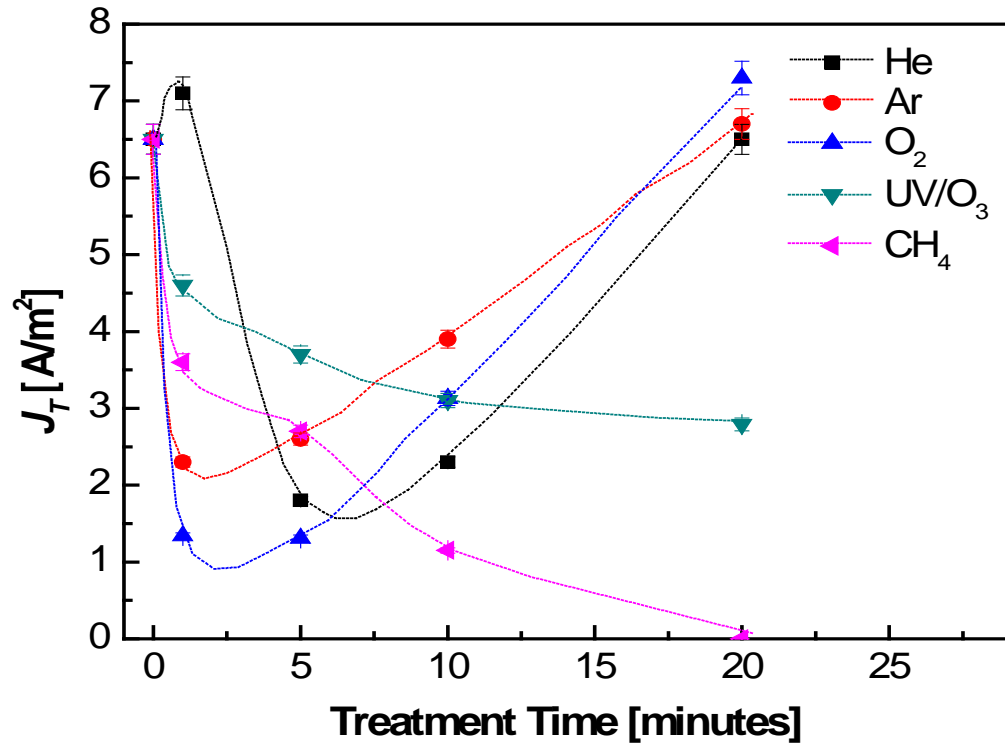
Fig 4.15. Variation of threshold current (J_T) with treatment time for c-Si/Alq$_3$/Al heterostructure.

J_T for the heterostructure with c-Si surface treated with CH$_4$ plasma decreased significantly with increase in treatment time as a result of the formation of a thin carbon layer on the c-Si layer. The decrease in J_T for the heterostructrue with UV/O$_3$ treated c-Si surface is mainly due to the incorporation of the O atoms into the c-Si surface. Long duration of He, Ar, and O$_2$ plasma treatments etches the SiO$_2$ layer on the c-Si surface which have the effect of increasing the J_T for the heterostructure.

4.3.10 OLED Driving Voltage: c-Si/Alq$_3$/Al Heterostructure
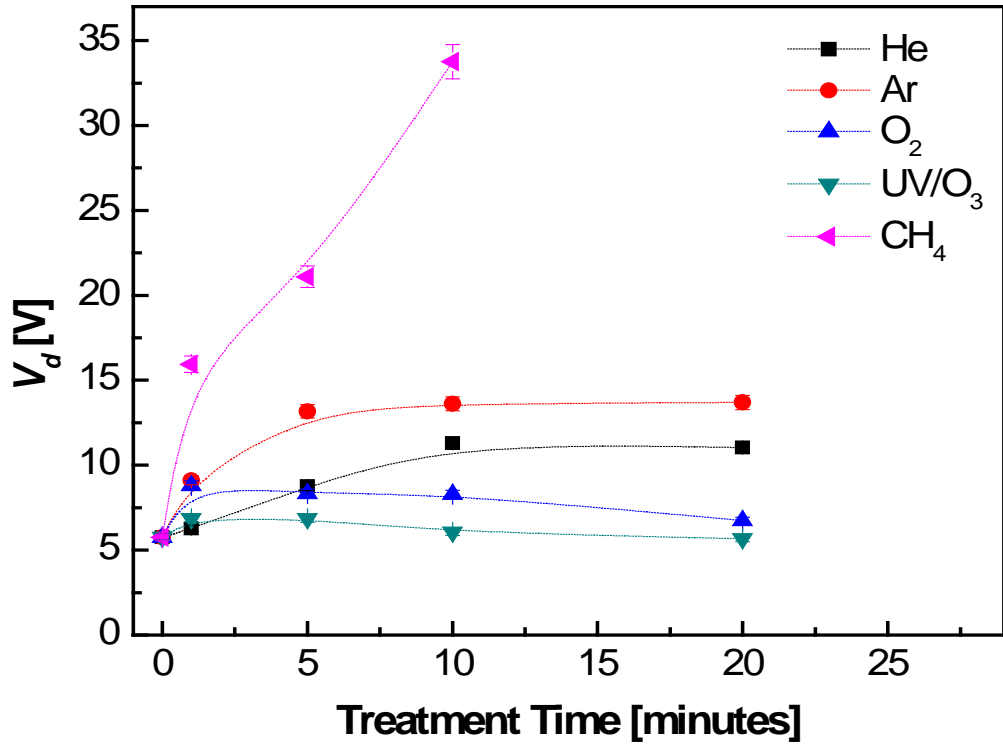
Fig 4.16. Variation of OLED driving voltage (V_d) with treatment time for c-Si/Alq$_3$/Al heterostructure.

The variation of V_d with treatment time for c-Si/Alq$_3$/Al heterostructure after the c-Si surface treatments using CH$_4$, He, Ar, O$_2$ plasma, and UV/O$_3$ treatment is shown in Fig. 4.16. The V_d value for CH$_4$ plasma treated c-Si heterostructure was very large and was beyond the measurement range carried out in this work when the treatment time was increased to 20 minutes. The lowest V_d of 5.7 V was obtained for the heterostructure with c-Si treated with UV/O$_3$ for 20 minutes. In general, all the V_d values for the plasma treated c-Si heterostructures were higher compared to the untreated c-Si heterostructure. This indicates that plasma treatment done on the c-Si heterostructure increased the V_d for c-Si based OLED devices.

CH$_4$ plasma treatment on the c-Si heterostructure significantly increases the V_d with the increase in treatment time as a result of formation of carbon layer on the c-Si surface. The lowering of the V_d value for the heterostructure with long duration of He, Ar, and O$_2$ plasma treated c-Si surface is a result of increasing ion bombardment effect with the increase in treatment time thus reducing the plasma cleaning effect. This results in an increase in structural defects instead of removing the hydrocarbon contaminations from the c-Si surface with increase in exposure of the c-Si to the plasma treatments. UV/O$_3$ treatment significantly lowered the V_d for the heterostructure as result of the incorporation of O atoms into c-Si surface. These results show that c-Si/Alq$_3$/Al heterostructure is not suitable for OLED device since the lowest V_d achieved is considered to be high for the turn-on voltage for OLED devices.

4.3.11 Fowler-Nordheim Plots of c-Si/Alq$_3$/Al Heterostructure

Fig. 4.17 shows the FN plots of c-Si/Alq$_3$/Al heterostructure after the c-Si surface treatments using CH$_4$, He, Ar, O$_2$ plasma, and UV/O$_3$ treatment. CH$_4$ plasma treatment on the c-Si substrates shifted the linear part of the FN plots to the higher field value while the linear part in the FN plots for the UV/O$_3$ treated heterostructure shifted to lower field with the increase in treatment time. He and Ar plasma treated c-Si surface shifted the linear part of the FN plots to the lowest field value when the treatment time was 1 minute while O$_2$ plasma treated c-Si surface shifted the linear part of the FN plots to the lowest field value when the treatment time was 5 minutes.
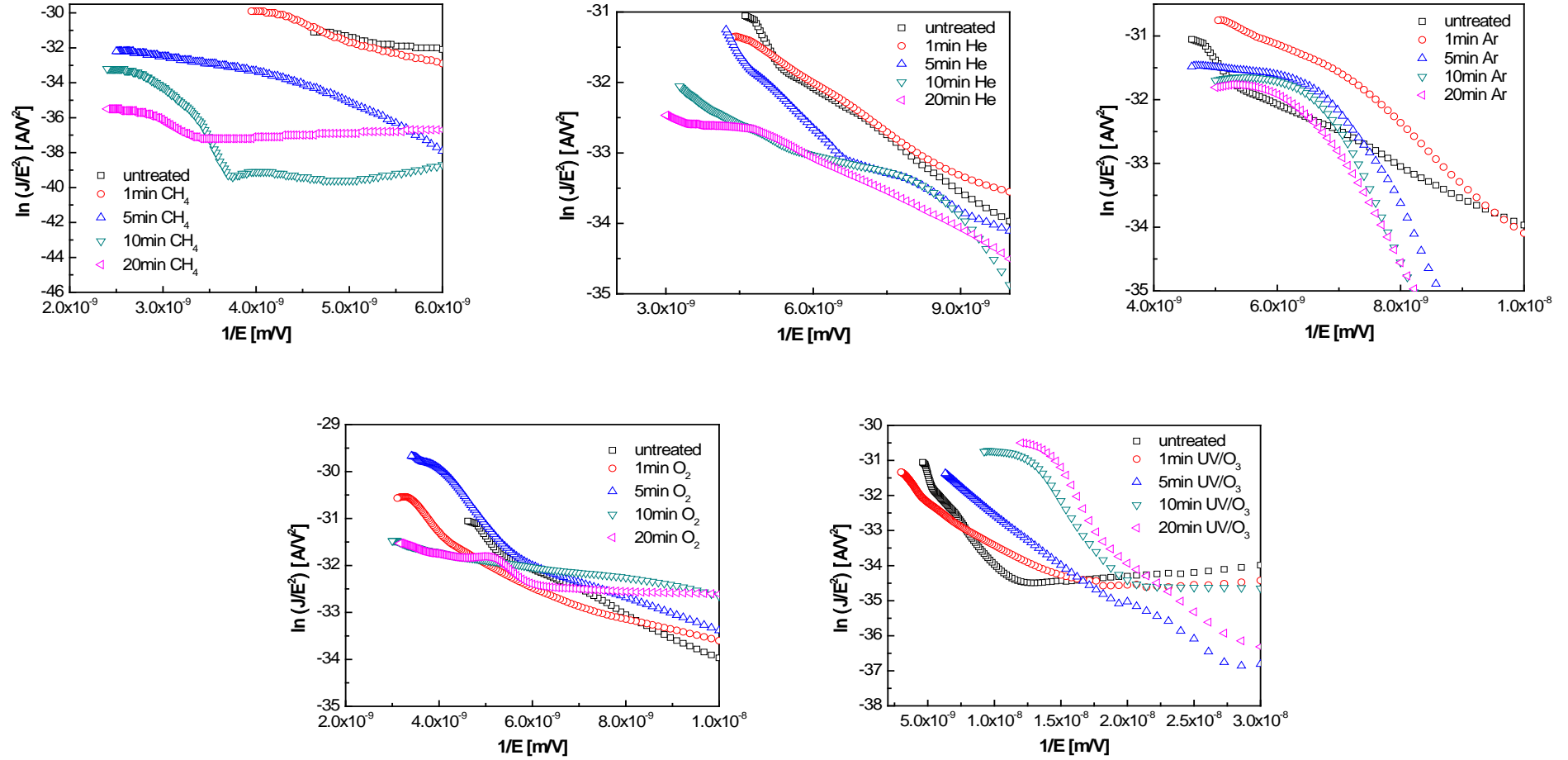
Fig. 4.17. Fowler-Nordheim plots for c-Si/Alq$_3$/Al heterostructure where the Alq$_3$ films were deposited on the untreated c-Si substrates and c-Si substrates treated with CH$_4$, He, Ar, O$_2$ plasma, and UV/O$_3$ treatment for 1, 5, 10, and 20 min, respectively.

4.3.12 Hole Injection Barrier: c-Si/Alq₃/Al Heterostructure
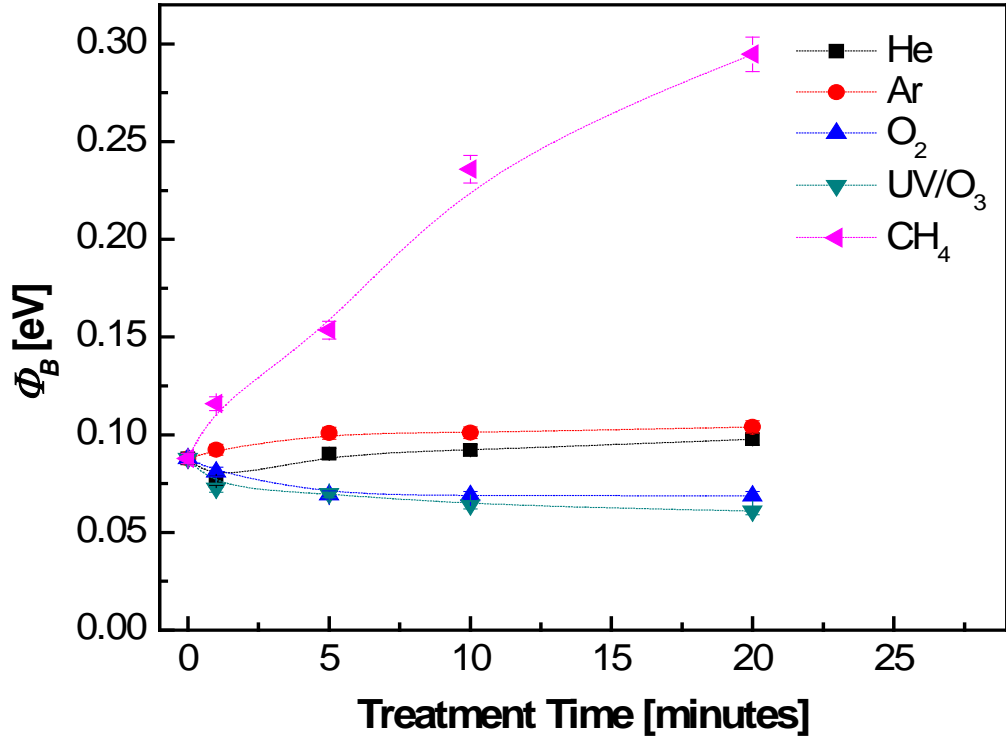
Fig 4.18. Variation of barrier height (Φ_B) with treatment time for c-Si/Alq₃/Al heterostructure.

Fig. 4.18 shows the variation of Φ_B with treatment time for c-Si/Alq₃/Al heterostructure with c-Si substrates untreated and treated with CH_4, He, Ar, O_2 plasma, and UV/O_3 treatment for 0, 1, 5, 10, and 20 minutes, prior to the Alq₃ film deposition. CH_4 plasma treatment on the c-Si heterostructure produced the highest Φ_B for the heterostructure compared to other treatments. Φ_B for the heterostructure with CH_4 plasma treated c-Si surface significantly increased from 0.09 to 0.3 eV with the increase in treatment time to 20 minutes. Both O_2 plasma and UV/O_3 treatments produced a decrease in Φ_B for the heterostructure with increase in treatment times. The lowest Φ_B of 0.06 eV was obtained from the UV/O_3 treated c-Si heterostructure followed by the O_2 plasma treated c-Si heterostructure with Φ_B value of 0.07 eV. He and Ar plasma

treatments produced no significantly change in Φ_B for the heterostructure; except for the 1 minute of He plasma treated c-Si heterostructure where Φ_B decreased to a minimum value of 0.08 eV.

Increase in Φ_B for the heterostructure with CH_4 plasma treated the c-Si surface is due to the formation of carbon film on the c-Si surface. Decrease in Φ_B for the heterostructure with UV/O_3 and O_2 plasma treatments on the c-Si surface is attributed to the incorporation of O atoms into the c-Si surface.

4.4 Discussion of Results

The results above showed the effects of CH_4, Ar, He and O_2 plasma treatment time on ITO and p-type c-Si on the PL properties of Alq_3 films deposited on these substrates. The influence of the treatment time of these substrates on the electrical properties of ITO/Alq_3/Al and p-type c-Si/Alq_3/Al heterostructures using the treated substrates as anode material are also presented. The effects of UV/O_3 treatment time of these substrates on these properties are also presented. This technique is the only non plasma based treatment technique studied in this work since it is a widely used technique for cleaning ITO in OLED applications.

CH_4 plasma treatment on the surface of ITO and c-Si substrates involves discharge of the gas producing radicals and hydrocarbon ions in the plasma. These radicals and ions have the effects of forming a layer of hydrocarbon film and bombarding the substrates surfaces respectively. The results above showed that the PL emission peak intensity of the Alq_3 film deposited on the ITO and c-Si substrates treated was degraded with increase in CH_4 treatment time. PL emission peak position of the Alq_3 film

deposited on the CH_4 plasma treated ITO significantly blue shifted due to the formation of a layer of hydrocarbon film at the interface which has a different structure from the ITO and Alq_3. CH_4 plasma treatment introduced impurities of C atoms into the c-Si surface that produced the red shift in the PL emission peak position.

This hydrocarbon layer formed as a result of CH_4 plasma treatment on the ITO surface acts as an additional energy barrier for holes injection. This reduces the injection of hole into the Alq_3 layer and also reduces the number of electrons reaching the anode. This increases V_T for the heterostructure. However, for the c-Si substrates, the native silicon oxide (SiO_2) present on the c-Si surface acts as an additional barrier for electrons moving to the anode since it is an insulator. This explains the higher V_T for c-Si/Alq_3/Al heterostructure compared to V_T for ITO/Alq_3/Al heterostructure. Reduction in hole injection certainly increase the V_T and this is reflected by the decrease in J_T with CH_4 plasma treated ITO and c-Si heterostructure. The increase in Φ_h is contributed by the decrease in the dipole moment at the interface, as a result of the increase of the hydrocarbon layer on the ITO and c-Si surface. The decrease in the dipole moment is due to the increase in the separation between the positive and negative charge accumulation on the anode material and Alq_3 side as the hydrocarbon layer thickness increases. The lower Φ_B for the c-Si/Alq_3/Al heterostructure is not expected as the band-diagram in Fig. 2.8 clearly shows that the hole injection barrier at c-Si/Alq_3 interface is much larger than the ITO/Alq_3 interface. However, the SiO_2 layer present on the c-Si surface increases the dipole moment at the c-Si/Alq_3 interface, thus reducing the hole injection barrier [Brutting, (2005)].

Both He and Ar plasma treatments have the cleaning effects as well as ion

bombardment effects during the plasma treatment [*Wu et al., (1997), Furukawa et al, (1997)*]. The cleaning effect is dominant with short duration of treatment time while the ion bombardment effect is dominant with long duration of treatment time. Comparatively, the ion bombardment effect by the Ar^+ ions are more destructive due to higher in mass compared to the He^+ ion.

Short duration of He and Ar plasma treatments on ITO and c-Si substrates enhances the PL emission peak intensity as a result of removal of hydrocarbon contaminants on the ITO and c-Si surface due to its cleaning effects. Long duration of He and Ar plasma treatments on the ITO and c-Si substrates produces longer duration of He^+ and Ar^+ ion bombardments on the ITO and c-Si. This is expected to produce defective structures on the ITO and c-Si surface as a result of the weakening and breaking of bonds between the atoms at the surface [*Ho, (2003, Cheng et al., (2006)*]. These ion bombardments also increase the surface roughness of the treated surface [*Chan et al., (2002)*]. The smaller mass of He^+ ions compared to Ar^+ ion explains the small change in the PL emission intensity for both Alq_3 film on ITO and c-Si substrates as a result of He plasma treatments.

The cleaning effects of short duration He and Ar plasma treatment reduces the V_T for the $ITO/Alq_3/Al$ and $c-Si/Alq_3/Al$ heterostructure. The removal of hydrocarbon layer increases the mobility of holes and this increase in J_T and decrease in V_d. This also explains the decrease in the Φ_h. However, long duration of He and Ar plasma treatment on the ITO and c-Si significantly increases the V_T for the $ITO/Alq_3/Al$ and $c-Si/Alq_3/Al$ heterostructure mainly due to the presence of structural defects on the surface produced by ion bombardments as reported in Ho [*Ho, (2003)*] and Cheng et al [*Cheng et al.,*

(2006)]. Increase in J_T for the c-Si/Alq$_3$/Al heterostructure for long duration He and Ar plasma treatment is mainly contributed by the removal of the SiO$_2$ layer on the c-Si surface. This SiO$_2$ layer also acts as a buffer layer that balance between the holes injected from anode and electrons from cathode [*Ma et al., (2006)*]. Consistently, V_T and V_d for He plasma treated ITO/Alq$_3$/Al and c-Si/Alq$_3$/Al heterostructures are lower compared to the V_d for Ar plasma treated ITO/Alq$_3$/Al and c-Si/Alq$_3$/Al heterostructures. The Φ_h for the c-Si/Alq$_3$/Al heterostructure is lower compared to ITO/Alq$_3$/Al heterostructure due to the presence of thin native SiO$_2$ layer on the c-Si surface that increases the dipole moment at the c-Si/Alq$_3$ interface. This effect is also observed in the case of CH$_4$ plasma treated c-Si heterostructure as discussed above.

PL emission peak intensity of the Alq$_3$ film deposited on the ITO and c-Si substrates treated with UV/O$_3$ was significantly enhanced with increase in treatment time. The incorporation of O atoms into the ITO and c-Si surface by the UV/O$_3$ treatment increased the concentration of O atoms at the interface thus enhancing the PL emission intensity. The PL emission intensity of the Alq$_3$ film on the c-Si substrates is significantly lower than the PL emission intensity of the Alq$_3$ films on ITO.

O$_2$ plasma treatment also produces sputtering effects on the ITO surface. The O$^+$ ion bombardments etched away the weak bonds on the ITO surface however O atoms are incorporated back into the ITO surface during O$_2$ plasma treatment. The shift in the PL emission peak positions are blue shifted with increase in UV/O$_3$ and O$_2$ plasma treatment time on the ITO surface. The shift is more significant in the UV/O$_3$ treatment as compared to O$_2$ plasma treatment. This is due to the higher concentration of O atoms incorporated into the ITO surface thus forming a stable oxide [*Lin et al., (2001)*].

O$_2$ plasma and UV/O$_3$ treatments on the ITO and c-Si significantly decrease V_T for the ITO/Alq$_3$/Al and c-Si/Alq$_3$/Al heterostructures. O$_2$ plasma treatment introduces oxygen into ITO surface increasing the work function [*Song et al., (2001)*] thus decreasing hole injection barrier Φ_h and enhancing the carrier injection [*Milliron et al., (2000)*]. The reduction of hydrocarbon layer by O$_2$ plasma treatment increases the hole injection ability at the ITO/Alq$_3$ interface. ITO in general is considered as a heavily doped and degenerate n-type indium oxide with both Sn dopants and oxygen vacancies contributing to its conduction [*Wu et al., (1997)*]. Thus, the enhancement of hole injection is due to the increase in the oxygen concentration by the O$_2$ plasma treatment. Treating the c-Si surface with O$_2$ plasma treatment forms a new layer of SiO$_2$ on the c-Si surface from the oxygen radicals in the plasma oxygen discharge. The passivation effect of the radical oxygen forms Si-O-Si bonds and this reduces the density of trap states and barrier potential [*Mitra et al., (1991)*]. The dissociation of the oxygen by the UV irradiation, results in the formation of ozone. The ozone assists the oxidation of the surface, to form a stable oxide – In$_2$O$_3$, thereby increasing the work function [*Lin et al., (2001)*].

Treating the ITO surface with UV/O$_3$ treatment also removes the hydrocarbon layer on the ITO surface. Reduction of hydrocarbon layer is equivalent to the reduction of barrier potential, which decreases hole injection barrier and increases the total amount of the injected carrier. However, long duration of O$_2$ plasma treatment prolongs ion bombardment effects on the treated surface. J_T for the c-Si/Alq$_3$/Al heterostructure increases after long duration of O$_2$ plasma treatment on the c-Si surface as a result of removal of SiO$_2$ buffer layer, leading to excessive of injected holes from the anode.

Chapter 5 Conclusions and Suggestions for Future Works

5.1 Conclusions

In this work, a thermal evaporation system has been successfully built for the deposition of Alq_3 films. The ITO and p-type c-Si surface which are used as substrates for these films are subjected to various surface treatments using CH_4, He, Ar, O_2 plasma and UV/O_3 treatment to investigate the photoluminescence and electrical properties.

From the photoluminescence results and analysis, the CH_4 plasma treatment on the ITO and c-Si surface produced a thin layer of hydrocarbon on the surfaces. The thickness of this hydrocarbon layer increases with increase in the treatment time. This hydrocarbon layer has the effect of decreasing the PL emission peak intensity and blue-shifting the peak position due to the incorporation of the impurities of C atoms.

The PL properties of Alq_3 films on ITO and c-Si substrates are affected with these inert gas plasma treatments on these substrates surfaces. Short duration of inert gas plasma treatments increases the PL emission intensity due to the cleaning effect by the removal of the hydrocarbon layer on the ITO and c-Si surface. However, long duration of inert gas plasma treatments decreases the PL emission peak intensity due to prolonged ion bombardment effects that is destructive to the ITO and c-Si surface and creates surface defect states on the ITO and c-Si surface.

For ITO and c-Si surface with O_2 plasma and UV/O_3 treatment, the PL emission intensity increases with increase in treatment time which is also due to the removal of the hydrocarbon layer on the ITO and c-Si surface. However, for long duration treatments, the PL emission intensities for film on O_2 treated ITO and c-Si substrates are lower than the PL intensity for UV/O_3 treated ITO and c-Si substrates. This is attributed

to the longer O^+ ion bombardments on the surfaces with long duration of O_2 plasma treatment.

From the results, Alq_3 films on c-Si substrates exhibits poor PL properties regardless of various surface treatments on the c-Si surface. The PL emission intensity of the Alq_3 films on the treated c-Si surface obtained is much lower than the PL emission intensity of the Alq_3 films on the treated ITO. Thus, it is not a suitable anode material for OLED device.

The electrical properties of the ITO/Alq_3 and c-Si/Alq_3/Al hetrostructures are either enhanced or degraded depending on the surface treatments done on the anode material. The lowest electronic quality heterostructures is obtained from CH_4 plasma treated ITO and c-Si heterostructures. CH_4 plasma treatment causes an increase in Φ_B due to the formation of a thin layer of hydrocarbon on the ITO and c-Si surface. This hydrocarbon layer also acts as an additional barrier that reduces the total amount of carrier injection and decreases the current density. The V_T for the ITO/Alq_3/Al and c-Si/Alq_3/Al heterostructure increases with CH_4 plasma treatment and this reduces J_T for the ITO/Alq_3/Al and c-Si/Alq_3/Al heterostructures.

Φ_B for the short duration inert gas plasma treated ITO/Alq_3/Al heterostructure is lower when compared to the untreated ITO heterostructure. This is due to the removal of the hydrocarbon layer on the ITO surface by the inert gas plasma cleaning effects. The Φ_B for the 1 minute He plasma treated c-Si/Alq_3/Al heterostructure is lower compared to the long duration of He and Ar plasma treated c-Si heterostructure. This is due to the longer exposure to ion bombardments on the c-Si surface which creates surface defects states that induces the increase in the the hole injection barrier.

Long duration of UV/O$_3$ treatment on the ITO and c-Si anode material produces the highest enhancement on the electrical properties of the heterostructures followed by O$_2$ plasma treatment. This is mainly due to the improvement in hole injection into the Alq$_3$ layer with increase in treatment time. The improvement in hole injection decreases both the Φ_B and V_T for ITO/Alq$_3$/Al heterostructures with increase in treatment time is the result of the increase in the ITO work function. The increase in J_T for ITO/Alq$_3$/Al heterostructure with UV/O$_3$ treatment and O$_2$ plasma treatment is also due to the improvement in hole injection. In the case of c-Si, Φ_B and V_T for c-Si/Alq$_3$/Al heterostructure decreases with increase UV/O$_3$ treatment time. However, for O$_2$ plasma treated c-Si heterostructure long duration treatment results in a slight increase in Φ_B and V_T for the heterostructure. This is due to the prolonged O$^+$ ion bombardments on the surface of the c-Si which results in structural defects on the surface.

5.2 Suggestions and Future Works

This work can be developed in the future to relate the PL and electrical properties of Alq$_3$ films on ITO and p-type c-Si anode treated with CH$_4$, He, Ar, O$_2$ plasma, and UV/O$_3$ treatment to the surface roughness of the treated surfaces using AFM (Atomic Force Microscope). Ultra-violet Photoelectron Spectroscopy (UPS) and X-ray Photoelectron Spectroscopy (XPS) can be used to study the formation of interfaces between organic and metal [*Blochwitsz et al., (2001), Gao and Kahn, (2003)*] to understand the origin of the dipole moments. This is important for the understanding of organic/metal interfaces and accurate description of the charge injection process across these interfaces. Besides, in order to improve the accuracy of the changes in the work

function after various surface treatments on the ITO and c-Si substrates, Kelvin probe method can be used to measure the surface potential or work function [*Harima et al., (2000), Hayashi et al., (2002)*]. This method is most suitable to provide correct results for band bending. The thermal deposition system can also be modified to make *in-situ* deposition and measurements [*Xu et al., (2006)*] to interconnect growth and analysis studies in ultra-high vacuum system [*Shen and Kahn, (2001)*]. Therefore, the deposited organic film can be transferred to the analysis system for analysis, and measurements can be done without breaking the vacuum. ITO and c-Si substrates properties will not be affected by the ambient as well as environment factors such as humidity, contaminants and dirts which could affect the device performance.

References

Alonso, M.I., Garriga, J.O., Osso, J.O., Schreiber, F., Barrena, E. and Dosch, H. (2003). J. Chem. Phys. **119**. 6335

Anthony, B., Breaux, L., Hsu, T., Banerjee, S. and Tasch, A. (1989). J. Vac. Sci. Technol. B. **7**. 621

Bao, Z., Lovinger, A.J. and Brown, J. (1998). J. Am. Chem. Soc. **120**. 207

Blochwitz, J., Fritz, T., Pfeiffer, M., Leo, K., Alloway, D.M., Lee, P.A. and Armstrong, N.R. (2001). Organic Electronics. **2**. 97

Borsenberger, P.M. and Weiss, D.S. (1993). *Organic Photoreceptors for Imaging Systems*: New York, M. Dekker

Braun, D., and Heeger, A.J. (1991). Appl. Phys. Lett. **58**. 1982

Brutting, W. (2005). *Physics of Organic Semiconductors*: Weinheim, Wiley

Burrows, P.E. and Forrest, S.R. (1993). Appl. Phys. Lett. **64**. 2285

Chen, I.M., Cheng, W.C. and Hong, F.C. (2002). Appl. Phys. Lett. **80 (1)**. 13

Cheng, Y.H., Lin, K.Y., Hung, Y.C., Cheng, C.H., Syao, K.C. and Lee, M.C. (2006). Appl. Surf. Sci. **252**. 6375

Chiang, C.K., Fincher, C.R., Park, Y.W., Heeger, A.J., Shirakawa, H. Louis, E.J., Gau, S.C. and MacDiarmid, A.G. (1977). Phys. Rev. Lett. **39**. 1098

Chiguvare, Z., Parisi, J. and Dyakonov, V. (2003). J. Appl. Phys. **94**. 2440

Choi, J.M., Jeong, S.H., Hwang, D.K., Im, S.G., Lee, B.H. and Sung, M.M. (2009). Organic Electronics. **10**. 199

Choi, K., Ghosh, S., Lim, J. and Lee, C.M. (2003). Appl. Surf. Sci. **206**. 355

Coter, F., Belaish, Y., Davidov, D., Ehrenfreund, E., McLean, M.R. and Nalwa, H.S. (1989). Synth. Met. **29**. E471

Dalton, L.R., Thomson, J. and Nalwa, H.S. (1987). Polymer. **28**. 543

Datta, D. and Kumar, S. (2010). Solar Energy Materials & Solar Cells. **94**. 420

Diani, M., Bischoff, J.L., Kubler, L. and Bolmont, D. (1992). Appl. Surf. Sci. **62**. 67

Dimitrakopoulos, C.D. and Mascaro, D.J. (2001). J. Res. Dev. **45**. 11

Do, L.M., Han, E.M., Yamamoto, N. and Fujihira, M. (1996). Thin Solid Films. **273**. 202

Donose, B.C., Taran, E., Vakarelshi, I.U., Shinto, H. and Higashitani, K. (2006). Journal of Colloid and Interface Science. **299**. 233

Dumas, P. and Chabal, Y.J. (1991). Chem. Phys. Lett. **181**. 537

Finne, R.M. and Kline, D.K.J. (1967). J. Electronchem. Soc. **114**. 965

Fukushi, Y., Kominami, H., Nakanishi, Y. and Hatanaka, Y. (2005). Appl. Sur. Sci. **244**. 537

Furukawa, K., Terasaka, Y., Ueda, H. and Matsumura, M. (1997). Synth. Metals. **91**. 99

Gao, W. and Kahn, A. (2003). J. Phys. Condens. Matter. **15**. S2757

Gutmann, F. and Lyons, L.E. (1967). *Organic Semiconductors*: John Wiley & Sons

Hadziioannou, G. and Hutten, van P.F. (2000). *Semiconducting Polymers: Chemistry, Physics and Engineering*: Weinheim, Wiley

Haines, W.G. and Bube, R.H. (1978). J. Appl. Phys. **49**. 304

Harima, Y., Yamashita, K., Ishii, I. and Seki, K. (2000). Thin Solid Films. **366**. 237

Hayashi, N., Ishii, H., Ouchi, Y. and Seki, K. (2002). J. Appl. Phys. **92**. 3784

Ho, J.J. (2003). Electron Lett. **39**. 5458

Houston, M.R. and Maboudian, R.J. (1995). J. Appl. Phys. **78**. 3801

Iso, S., Igarashi, T. and Matsuno, H. (1999). J. Illum. Eng. Jpn. **83**. 273

Jeong, C.H., Lee, J.H., Lim, J.T., Kim, M.S. and Yeom, G.Y. (2007). Surf. & Coat. Tech. **201**. 5012

Kafader, U., Sirringhaus, H. and Kanel, H.V. (1995). Appl. Surf. Sci. **90**. 297

Kampen, T.U., Salvan, G., Friedrich, M., Tenne, D.A., Park, S. And Zahn, D.R.T. (2000). Appl. Surf. Sci. **166 (1-4)**. 387

Kawabata, Y. and Adachi, S. (1999). Appl. Surf. Sci. **152**. 177

Keithley Instrument Inc. Model 236 Source Measure Unit Instruction Manual. (1989). USA

Kim, J.S., Granstrom, M., Friend, R.H., Johanson, N., Salaneck, W.R. and Cacialli, F. (1998). J. Appl. Phys. **84**. 6859

Klaus, M. and Ullrich, S. (2006). *Organic Light Emitting Devices: Synthesis, Properties and Applications*: German, Wiley

Koezuka, H., Tsumara, A. and Ando, T. (1987) Synth. Met. **18**. 699

Kosugi, R., Ichimura, S., Kurokawa, A., Koike, K., Fukuda, K., Suzuki, S., Okushi, H., Yoshida, S. and Arai, K. (2000). Appl. Surf. Sci, **159**. 550

Krusor, B.S., Biegelson, D.K., Yingling, R.D. and Abelson, J.R. (1986). J. Vac. Sci. Technol. B. **7**. 129

Kumar, S. Shukla, V.K. and Tripathi, A. (2005). Thin Solid Films. **477**. 240

Laudise, A., Kloc, C., Simpkins, P. and Siegriest, T. (1998). J. Cryst. Growth. **187**. 449

Levenets, V.V., Beklemishev, V.I., Kirilenko, E.P., Makhonin, I.I., Trifonov, A.Yu., Loginov, B.A. and Protasenko, V.V. (1995). **34**. 1723

Li, C.N., Kwong, C.Y., Djurisic, A.B., Lai, P.T., Chui, P.C., Chan, W.K. and Liu, S.Y. (2005). Thin Solid Films **477**. 57

Li, F., Tang, H., Shinar, J., Resto, O. and Weisz, S.Z. (1997). Appl. Phys. Lett. **70**. 2741

Li, Z.G. and Meng, H. (2006). *Organic Light-Emitting Materials and Device*s: Delaware, CRC Press

Lin, H. N., Chen, S.H., Perng, G.Y. and Chen, S.A. (2001). J. Appl. Phys. **89**. 3976

Liu, H.H., Yan, F., Li, W.L., Lee, C.S., Chu, B., Chen, Y.R., L, X., Han, L.L., Su, Z.S., Zhu, J.Z., Kong, X.G., Zhang, L.G. and Luo, Y.S. (2010). Organic Electronics. **11**. 946

Ma, G.L., Ran, G.Z., Zhao, W.Q., Xu, Y.H., Qiao, Y.P., Zhang, B.R., Dai, L. and Qin, G.G. (2006). Semicond. Sci. Technol. **21**. 740

Ma, G.L., Xu, A.G., Ran, G.Z., Qiao, Y.P., Zhang, B.R., Chen, W.X., Dai, L. and Qin, G.G. (2006). Thin Solid Films. **496**. 665

Mason, M.G., Hung, L.S., Tang, C.W., Lee, S.T., Wang, K.W. and Wang, M. (1999). J. Appl. Pyhs. **86**. 1688

McElvain, J., Antoniadis, H., Hueschen, M.R., Miller, J.N., Roitman, D.M., Sheats, J.R. and Moon, R.L. (1996). J. Appl. Phys. **80**. 6002

Milliron, D.J., Hill, I.G., Shen, C., Kahn, A. and Schwartz, J. (2000). J. Appl. Phys. **87**. 572

Mitra, U., Chen, J., Khan, B. and Stupp, (1991). E. IEEE Electron Devices Lett. **12 (7)**. 390

Niimi, H. and Lucovsky, G. (1999). J. Vac. Sci. Technol. A **17**. 3185

Nuesch, F., Forsythe, E.W., Le, Q.T., Gao, Y. and Rothberg, J. (2000). J. Appl. Phys. **87**. 7973

Pan, L.K. and Sun, Z. (2009). Current Applied Physics. **9**. 1351

Park, Y., Choong, V., Gao, Y., Hsieh, B.R. and Tang, C.W. (1996). Appl. Phys. Lett. **68**. 2699

Park, Y.B., Kang, J.K. and Rhee, S.W. (1996). Thin Solid Films **280**. 43

Parker, I.D. (1994). J. Appl. Phys. **75**. 165

Parker, I.D. and Kim, H.H. (1999). Appl. Phys. Lett. **64**. 1774

Perkin-Elmer Luminescence Spectrometer LS50B User Manual

Pope, M. and Swenberg, C.E. (1982). *Electronic Processes in Organic Crystals*: Clarendon Press, Oxford

Priestley, R., Sokolik, I., Walser, A.D., Tang, W.C. and Dorsinville, R. (2002). Synth. Met. **84**. 72

Purvis, K.L., Lu, G., Schwartz, J. and Bernasek, S.L. (2000). J. Am. Chem. Soc. **122**. 1808

Ramm, J., Beck, E. and Zueger, A. (1991). Mater. Res. Soc. Symp. Proc. **220**. 15

Ramm, J., Beck, E., Zueger, A. Dommann, A. and Pixley, R.E. (1994). **222**. 158

Ran, G.Z., Xu, Y.H., Ma, G.L., Xu, A.G., Qiao, Y.P., Chen, W.X. and Qin, G.G. (2005). Semicond. Sci. Technol. **20**. 761

Rogers, J.A., Bao, Z., Dodabalapur, A. and Makhija, A. (2000). IEEE Electron Device Lett. **21**. 100

Schroder, D.K. (1998). *Semiconductor Material and Device Characterization*: New York, Wiley

Shaw, J.M. and Seidler, P.F. (2001). J. Res. Dev. **45**. 3

Shen, C.F. and Kahn, A. (2001). Organic Electronics. **2**. 89

So, S.K., Choi, W.K., Cheng, C.H., Leung, L.M. and Kwong, C.F. (1999). Appl. Phys. A **68**. 477

Song, W., So, S.K. and Cao, L. (2001). Appl. Phys. A **72**. 361

Song, W.J., So, S.K., Wang, D.Y., Qiu, Y. and Gao, L. (2001). Appl. Surf. Sci. **177**. 158

Suemitsu, M., Kaneko, T. and Miyamoto, N. (1989). Jpn. J. Appl. Phys. **28**. 2421

Sze, S.M., (1981). *Physics of Semiconductor Devices*: New York, Wiley

Takahagi, T., Nagai, I., Ishitani, A., Kuroda, H. and Nagasawa, Y. (1988). J. Appl. Phys. **64**. 3516

Tang, C.W. (1986). Appl. Phys. Lett. **48**. 183

Tang, C.W. and Vanslyke, S.A. (1987). Appl. Phys. Lett. **51**. 913

Tang, C.W. and Vanslyke, S.A. (1989). J. Appl. Phys. **65**. 3610

Tomita, N., Kawabata, Y. and Adachi, S. (2000). Mater. Sci. Eng. B. **68**. 175

Wu, C.C., Wu, C.I., Sturn, J.C. and Kahn, A. (1997). Appl. Phys. Lett. **70**. 11

Wu, C.C., Wu, C.I., Sturn, J.C. and Kahn, A. (1997). Appl. Phys. Lett. **70**. 1348

Xu, X.M., Wu, J.H., Wang, H., Wu, C.D., Ye, J.H., Wu, A.J., Qu, S. and Peng, J.C. (2007). Trans. Nonferrous Met. Soc. China. **17**. 1117

Xu, Y.F., Zhang, H.Y., Li, H.Y., Bao, S.N. and He, P. (2006). Appl. Sur. Sci. **252**. 2328

Yeates, A.T., Dudis, D.S. and Connolly, J.W. Snyth. Met. **116**. 289.

Yu, H.Y., Feng, X.D., Grozea, D., Lu, Z.H., Sodhi, R.N., Hor, A.M. and Aziz, H. (2001). Appl. Phys. Lett. **78**. 2595

Zhou, X., He, J., Liao, L.S., Lu, M., Xiong, Z.H., Ding, X.M., Hou, X.Y., Tao, F.G., Zhou, C.E. and Lee, S.T. (1999). Appl. Phys. Lett. **74**. 609

Appendix A: Home-Built Thermal Evaporation System

Fig. A.1. Home-Built Thermal Evaporation System

The evaporation chamber is made of stainless steel. The evaporation chamber consists of a stainless steel cylinder tube with top and bottom stainless steel plate attached to it. The vacuum o-ring is used at both sides to prevent leakage when the evaporation chamber is pumped down. The top plate supports the substrate holder, open/close shutter feed-through and air admittance valve while the bottom plate supports the electrical lead-through for the current supply system, thermocouple, quartz

thickness monitor sensor feed-through and the pressure gauge (Pirani and Penning gauge). Inside the chamber there is a alumina crucible boat which is held by the tungsten wire. Deposition process takes place in the evaporation chamber.

In this home-built thermal evaporation system, rotary vane and turbo pump are used as the pumping system to evacuate the evaporation chamber to a desired pressure of $\sim 8 \times 10^{-6}$ mbar. The pressure in the system is measured using the Pirani (low vacuum) and Penning (high vacuum) gauge which are attached directly to the evaporation chamber. The quartz thickness monitor sensor is used to monitor the deposition rate and desired thickness of the deposited film. The current supply system provides the current through the electrical lead-through that head up the tungsten and alumina crucible boat.

Appendix B: Error Analysis

B.1 Standard Deviation

Standard deviation

$$\Delta S = \left[\frac{\sum\limits_{i=1}^{N}\left(x_i - \overline{x}\right)^2}{N\left(N-1\right)} \right]^{1/2}$$

where x_i, $\overline{x}$ and N are data, mean data, and number of data respectively.

B.2 Standard Error

Consider S as a function of variables of x, y,…

where $S = f\left(x, y, ...\right)$

The standard error, ΔS, is

$$\frac{\Delta S}{S} = \sqrt{\left(\left(\frac{\Delta x}{x}\right)^2 + \left(\frac{\Delta y}{y}\right)^2 + ...\right)}$$

where x, y,…… is various variable

Appendix C: Papers and Publications

1. J.Y. Koay, Khairul Anuar M. Sharif and Saadah A. Rahman, **"Influence of Film Thickness on the Structural, Electrical and Photoluminescence Properties of Vacuum Deposited Alq$_3$ Thin Films on c-Silicon Substrate"**, Thin Solid Films, Volume 517, Issue 17, 1 July 2009, Pages 5298-5300